Time-Dependent Density Functional Perturbation Theory

New algorithms with applications to molecular spectra

Thesis submitted for the degree of

Doctor Philosophiæ

Candidate:

Dario Rocca

Supervisors:

Prof. Stefano Baroni

Dr. Ralph Gebauer

October 2007

Contents

Introduction

Since its first appearance in the mid 60s, Density Functional Theory (DFT) [1, 2] has demonstrated a strong predictive power in the study of ground-state properties and its popularity has grown largely in the years both in the condensed matter physics and in the quantum chemistry communities. This success is due to the good compromise between low computational cost and fair accuracy. The first is achieved by mapping the quantum many-body problem onto an independent electron one; the second is due to the success of simple approximations, such as Local Density Approximation (LDA), which work well beyond the range of validity originally foreseen on pure theoretical grounds. Nevertheless the broad class of problems related to excited states cannot be addressed by standard DFT. This field basically includes the study of all optical properties of molecules and solids, both in the linear or non-linear regimes.

The extension of DFT to deal with the time-dependent Schrödinger equation and excited-state properties has been achieved with the formulation of Time-Dependent Density Functional Theory (TDDFT) [3], a theory which has been mathematically established by the theorem of Runge and Gross [4]. In this approach the complex many-body time-dependent Schrödinger equation is replaced by a set of (coupled) time-dependent single-particle equations. For this reason this method is computationally much more suitable than cumbersome many body techniques to calculate optical spectra [5] and, in practice, it is the only possible choice in order to treat strongly non-linear phenomena in realistic systems. Furthermore, for many applications, very simple approximations to TDDFT, such as the adiabatic LDA (ALDA) [6], have shown an unexpected accuracy. These features have led to an incredibly rapid growth of this field in the last few years, as shown in Fig. 1.

The range of applications of TDDFT is wide but the greatest part of them

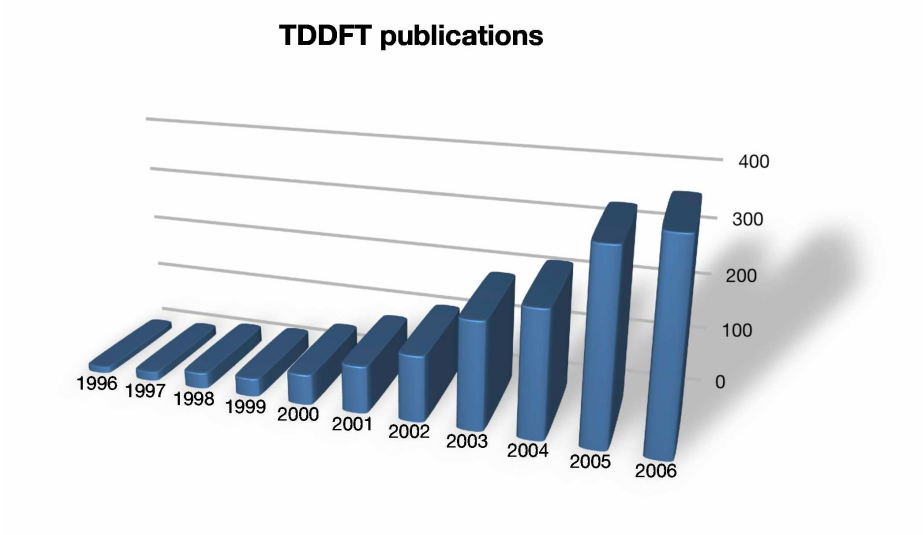

Figure 1: Publications per year based on TDDFT. These data have been obtained by searching the ISI Web of Science database with the "Time dependent density functional theory" and "TDDFT" keywords.

concerns the calculation of optical spectra of molecules and solids in the dipole approximation. Because of the huge dimension of this research area, we can only give a flavor of the problems addressed. There are applications to biochromophores, such as chlorophyll, the molecule responsible for the photosynthetic process [7, 8, 9, 10], the green fluorescent protein chromophore, which is an important molecular marker [11], and retinal, the molecule responsible for vision [12]. Still in the biological area there are studies of DNA bases [13] and of ruthenium complexes used as spectroscopic probes for DNA [14]. Much interest has been attracted by the optical properties of fullerenes, both in the spherical and nanotube form [15, 16, 17, 18, 12, 19, 20, 21] and of nanoclusters, both metallic and covalent [22, 23, 24, 25, 26, 27, 28, 29]. TDDFT can also be useful to address problems of strong applicative interest, such as dye-sensitized solar cells [30, 31]. The methodology has been extended in order to deal with circular dichroism as well [32, 33].

For what concerns the photo-absorption spectra of solids or low dimensional extended systems, such as nanostructures or long polymers, the predictive power of TDDFT is not as established. Indeed, for these systems the ALDA in general is no longer adequate. One of the most evident failures concerns its application to

semiconductors and insulators, since there is not a significant correction over the random-phase approximation results and excitonic effects are totally missed. Another well-known failure is the overestimate of polarizability in long conjugated molecules. Research to improve upon the limitations of ALDA (but also of other common local adiabatic approximations) to treat extended systems is extremely active and functionals derived from many-body theory have shown promising results [5, 34, 35, 36, 37, 38, 39, 40].

Besides the problem of excitons in solids, there are other well-known failures of TDDFT in the adiabatic approximation. In atom and molecules, Rydberg series are not reproduced since the corresponding states are usually unbound; this is due to the incorrect asymptotic behavior of the ALDA exchange-correlation potential, which does not describe properly the electron-hole interaction. Another well known failure concerns the charge transfer excitations, which are typically predicted too low in energy (sometimes by more than 1 eV). This problem is particularly dramatic when these transitions take place between weakly bound systems. Multiple excitations are completely missed in linear-response adiabatic TDDFT. The known failures of TDDFT and the attempts to solve them are reviewed in [41].

We finally mention that linear-response TDDFT can be used to approximate the exchange-correlation energy of the ground-state DFT problem, using the adiabatic-connection fluctuation-dissipation formula [42, 43]. In this framework properties such as van der Waals interactions, missed by standard ground-state functionals, are naturally included [44]. This methodology has been applied to calculate the correlation energy of the uniform electron gas [45], to reproduce the dissociation curve of small dimers [46], and to describe layered materials [47].

To cope with such a wide range of applications, different practical implementations of linear response TDDFT are available. In its most general form, the TDDFT linear response problem can be expressed in terms of a Dyson-like equation [48]. This equation allows to compute a generalized susceptibility, whose poles are excitation energies of the system under investigation. Through this response function it is possible to calculate the linear response of any local observable to any local external perturbation. The polarizability, which gives the optical absorption spectra, can also be obtained in this way. Nevertheless, since in general the computational cost of constructing and solving the Dyson-like problem is

very high, there are more efficient and widespread ways to solve TDDFT equations when only optical properties are required.

The Dyson-like equation for susceptibility has been reformulated by Casida [49] into an eigenvalue problem, whose eigenvalues and eigenvectors are used to build the optical absorption spectra. The construction of Casida's equations requires the prior diagonalization of the full ground-state problem; this operation may be very demanding, especially for large basis sets. The eigenvalue problem is then efficiently solved by iterative techniques [50, 51]. Nevertheless, within this approach only a limited number of the low-lying eigenvalues can be obtained. This leads to a limitation of the energy range accessible. Furthermore, the density of excitation energies in a given energy range increases linearly with the system size, thus making it difficult if not impossible to calculate them individually for very large systems.

Some of the drawbacks of Casida's approach have been overcome by directly solving the TDDFT equations in the time domain. For linear response purposes it is necessary to integrate this equations by adding a properly chosen small external perturbing potential [18, 12]. This method is suitable to calculate the optical spectra in a large energy range and the full diagonalization of the ground-state Hamiltonian is completely avoided, since it is necessary to propagate the occupied states only. The basic operations required to integrate TDDFT equations are the same as an iterative ground-state calculation; unfortunately they have to be performed many more times. For this reason the overall scalability of this method is basically the same as that of a ground-state calculation, but the prefactor is much larger.

From this general overview of TDDFT it results that there are two main open issues for a wide applicability of this methodology. One is related to the accuracy of the available xc functionals, which has to be improved in order to treat, e.g., excitons in solids or Rydberg states in finite systems. The other concerns the enhancement of the algorithmic performance of the method, which is essential for the application of TDDFT to realistic systems; indeed we need to build large models to simulate, e. g., biochromophores embedded in their biological environment or dye-sensitized solar cells, just to mention two important examples. In this thesis we will deal with this second issue. We will introduce a new approach to solve TDDFT equations in the linear regime, which can reach a performance com-

parable with ground-state calculations and which improves substantially upon the already good scalability of the real-time approach. This result will be achieved through the introduction of a formalism borrowed from time-independent density functional perturbation theory [52, 53, 54]. The resulting equations will then be solved using the Lanczos algorithm and an efficient extrapolation scheme to accelerate its convergence. After testing the method against molecular systems of increasing dimension (benzene, fullerene, and chlorophyll) we will address a problem of paramount current interest: dye-sensitized solar cells (DSSC's) [55]. These devices represent a particularly promising approach to the direct conversion of light into electrical energy at low cost and with high efficiency. In DSSC's, a dye sensitizer absorbs the solar radiation and transfers the photoexcited electron to a wide band-gap semiconductor electrode, while the concomitant hole is transferred to an electrolyte. Various ruthenium complexes have been successfully applied as sensitizers, obtaining efficiencies of about 10%. Research to further improve over such performance is extremely active. For this purpose it is necessary to find dyes with an absorption band that fit better to the solar spectrum or to apply different molecules as cosensitizers. In this thesis we will consider the specific case of a squaraine dye, which is a promising candidate for the red/near infrared sensitization. We will analyze the optical properties of a DSSC built with such molecule and we will investigate the mechanism ruling the functioning of the device.

This thesis is organized as follows. In Chapter 1 we will illustrate the basic concepts of DFT and TDDFT; the most common computational approaches will be also considered. In Chapter 2 our new formalism will be introduced together with the numerical algorithm and a first application to benzene. In chapter 3 we will illustrate a technique for extrapolating the Lanczos coefficients and to accelerate the convergence of the method. The resulting methodology will be applied to more challenging problems, such as fullerene and chlorophyll spectra. In Chapter 4 the method will be applied to the study of dye-sensitized solar cells. In appendix A and B we will give the technical details of our specific implementation in the plane-wave pseudopotential framework.

Chapter 1

Time-Dependent Density Functional Theory

In this chapter we will illustrate the theoretical background that underlies the work presented in this thesis. We will start by a short review of ground-state DFT and then introduce the basics of Time-Dependent Density Functional Theory (TDDFT) and its common practical implementation schemes.

1.1 Density Functional Theory

Density Functional Theory (DFT) is remarkably widespread in the condensed matter physics and quantum chemistry communities because of its good balance between accuracy and computational cost. The main (formidable) achievement of this approach is the mapping of a many-body electronic problem onto a non-interacting one. DFT was developed in the work of Hohenberg and Kohn [1] and in the work of Kohn and Sham [2]. Hohenberg and Kohn (HK) established the two theorems which constitute the theoretical foundation of DFT:

- **Theorem I**: For any system of interacting electrons in an external potential $v_{ext}(\mathbf{r})$, there is a one-to-one (apart from an irrelevant additive constant) correspondence between $v_{ext}(\mathbf{r})$ and the ground-state particle density, $n_0(\mathbf{r})$;
- **Theorem II**: The energy of an interacting-electron system in an external potential $v_{ext}(\mathbf{r})$ can be expressed as a functional of the electronic density,

$n(\mathbf{r})$, of the form

$$E_{HK}[n] = F_{HK}[n] + \int v_{ext}(\mathbf{r})n(\mathbf{r})d\mathbf{r}, \tag{1.1}$$

where $F_{HK}[n]$ is a universal functional of the density which does not depend on $v_{ext}(\mathbf{r})$. Furthermore, $E_{HK}[n]$ is minimal at the exact ground-state density $n_0(\mathbf{r})$, and its minimum gives the exact ground-state energy of the system.

The meaning of the first theorem is that the density completely determines all the properties of a given many body system. The second theorem is simply a corollary of the first and of the variational principle of quantum mechanics. The HK theorems provide a quite general theoretical result but they do not contain any recipe about how to solve the quantum many-body problem in practice.

A practical formulation of DFT is provided by the Kohn-Sham (KS) ansatz, which results in rewriting Eq. (1.1) as:

$$E_{HK}[n] = T_0[n] + E_H[n] + E_{xc}[n] + \int v_{ext}(\mathbf{r})n(\mathbf{r})d\mathbf{r}. \tag{1.2}$$

In Eq. (1.2) T_0 is the F_{HK} functional for a system of non-interacting electrons, coinciding therefore with its kinetic energy; the Hartree energy, $E_H[n]$, is the electrostatic self-energy of a classical charge-density distribution, $n(\mathbf{r})$:

$$E_H[n] = \frac{1}{2}\int\int \frac{n(\mathbf{r})n(\mathbf{r}')}{|\mathbf{r}-\mathbf{r}'|}d\mathbf{r}d\mathbf{r}'; \tag{1.3}$$

E_{xc} is finally *defined* by Eq. (1.2) as the difference $F_{HK}[n] - T_0[n] - E_H[n]$. In order to apply DFT in practice, a good approximation for E_{xc} is necessary; this problem will be addressed in the next section. By applying the variational principle of Theorem II to the HK energy functional in the form of Eq. (1.2) we obtain the Euler equation

$$\frac{\delta T_0[n]}{\delta n(\mathbf{r})} + v_{KS}(\mathbf{r}) = \mu, \tag{1.4}$$

where

$$\begin{aligned} v_{KS}(\mathbf{r}) &= v_H(\mathbf{r}) + v_{xc}(\mathbf{r}) + v_{ext}(\mathbf{r}) & (1.5)\\ &= \int \frac{n(\mathbf{r}')}{|\mathbf{r}-\mathbf{r}'|}d\mathbf{r}' + \frac{\delta E_{xc}[n]}{\delta n(\mathbf{r})} + v_{ext}(\mathbf{r}), & (1.6) \end{aligned}$$

and μ is a Lagrange multiplier that enforces the conservation of the total number of particles. The same equation (1.4) can be obtained by applying the variational principle to a system of non-interacting electrons in an external potential $v_{KS}(\mathbf{r})$. For this reason the ground-state density of the interacting-electron system, $n_0(\mathbf{r})$, can be obtained by solving the Schrödinger equation of a fictitious non-interacting system:

$$\left[-\frac{1}{2}\nabla^2 + v_{KS}(\mathbf{r})\right]\phi_i(\mathbf{r}) = \varepsilon_i\phi_i(\mathbf{r}). \tag{1.7}$$

The one-particle orbitals ϕ_i can be then used to construct the density

$$n(\mathbf{r}) = \sum_i^{N_v} \phi_i^*(\mathbf{r})\phi_i(\mathbf{r}), \tag{1.8}$$

where N_v is the number of occupied states. Eq. (1.7) is named Kohn-Sham equation. Since v_{KS} is a functional of the exact ground-state density, Eq. (1.7) has to be solved self-consistently. It is worth to note that, strictly speaking, the eigenvalues ε_i and eigenvectors ϕ_i do not have any physical meaning, but they are just mathematical devices used to obtain the ground-state energy and charge density of the full many-body system. Within this approach it is possible to calculate many ground-state properties; among them we mention atomic forces, equilibrium geometries, stress tensors and phonon dispersion curves.

1.2 Approximations for the exchange-correlation functional

The KS equation holds independently of any approximation on the functional $E_{xc}[n]$, thus it would give the exact ground-state properties of an interacting system if the exact functional was known. In practice the success of DFT is due to the fact that $E_{xc}[n]$ can be reasonably approximated by a local or nearly local functional of the density. The first and most widespread approximation to $E_{xc}[n]$ is the Local Density Approximation (LDA), which assumes that the xc energy of a real system behaves locally as that of a uniform electron gas. The xc functional in this case can be expressed as

$$E_{xc}^{LDA}[n] = \int \varepsilon_{xc}^{hom}(n(\mathbf{r}))n(\mathbf{r})d\mathbf{r}, \tag{1.9}$$

where $\varepsilon_{xc}^{hom}(n)$ is the xc energy per electron of the homogeneous electron gas at density n. The exchange contribution can be evaluated analytically [56], while the correlation part has been obtained by parameterizing the results of Monte Carlo simulations [57, 58, 59]. The LDA is exact in the limit of high density or of slowly varying density distributions; in fact experience has shown that accurate results are obtained well beyond this theoretical range of validity. Typically LDA yields a good accuracy in reproducing experimental structural and vibrational properties of strongly bound systems; it usually overestimates bonding energies and underestimates bond lengths. As a first improvement beyond LDA, the Generalized Gradient Approximation (GGA) has been introduced:

$$E_{xc}^{GGA}[n] = \int \varepsilon_{xc}^{GGA}(n(\mathbf{r}), |\nabla n(\mathbf{r}|) n(\mathbf{r}) d\mathbf{r}, \tag{1.10}$$

which depends also on the norm of the local density gradient, $|\nabla n(\mathbf{r})|$. Several expressions for ε_{xc}^{GGA} have been considered. The three most popular parametrizations are that of Becke (B88) [60], Perdew and Wang (PW91) [61], and Perdew, Burke, and Enzerhof (PBE) [62]. GGA significantly improves upon LDA to predict the binding energies of real materials.

In this work we will use only LDA and GGA functionals. There are other types of xc functionals which are explicitly orbital-dependent; among them we mention the self-interaction correction (SIC) methods, the Optimized Effective Potential (OEP), the Exact Exchange (EXX) and hybrid functionals such as B3LYP (for a review see [56]). Some of these functionals provide a remarkable improvement of the accuracy for some systems, but in general they also introduce a significant increase of the computational cost.

1.3 Time-Dependent Density Functional Theory

The main limit of standard DFT is that it is a ground-state theory, thus not strictly applicable to the calculation of excitation energies or other excited-state properties. A quite general and powerful method that avoids this difficulty in a DFT-like framework is Time-Dependent Density Functional Theory (TDDFT). This approach is basically an extension of the standard ground-state DFT to deal with time-dependent external perturbations. Clearly, the solution of this problem is re-

lated to the calculation of excitations, since the presence of a time-dependent external potential drives the system away from its stationary ground-state to higher energy levels. Individual excitation energies can be computed using TDDFT together with linear response theory (see Secs. 1.5 and 1.6). The rigorous mathematical foundation of TDDFT dates back to the work of Runge and Gross [4]. Here we summarize their results in a way that emphasizes the similarity with the conceptual structure of ground-state DFT:

- **Theorem I**: For any system of interacting electrons in an external time-dependent potential $v_{ext}(\mathbf{r}, t)$, which can be expanded in Taylor series with respect to time, and given an initial state $\Psi(t_0) = \Psi_0$, there is a one to one (apart from a trivial function of time only) correspondence between $v_{ext}(\mathbf{r}, t)$ and the time dependent particle density $n(\mathbf{r}, t)$;

- **Theorem II**: If we define the action integral

$$A = \int_{t_0}^{t_1} \langle \Psi(t) | i\frac{\partial}{\partial t} - \hat{H}(t) | \Psi(t) \rangle, \tag{1.11}$$

  then A can be expressed as a functional of the density

$$A[n] = S[n] - \int_{t_0}^{t_1} \int n(\mathbf{r}, t) v_{ext}(\mathbf{r}, t) dt d\mathbf{r}, \tag{1.12}$$

  where $S[n]$ is a universal functional of the time-dependent density (namely it does not depend on the external potential) and $A[n]$ is stationary for variations around the exact density of the system.

Similarly to ground-state DFT, the first theorem states that we can consider the electronic density (which is in this case time-dependent) as the fundamental variable that determines all the properties of the system. It is important to notice that, differently from DFT, in this case it is necessary to set an initial condition, since we are following an evolution in time. In TDDFT the variational principle cannot be formulated in terms of the energy as in Eq. (1.1), but it is necessary to introduce the action functional $A[n]$ (Theorem II). It can be easily shown that Eq. (1.11) is stationary in correspondence with the exact solution of the many-body time-dependent Schrödinger equation; for this reason the functional of Eq. (1.12) is stationary for the exact time-dependent density.

If we call $S_0[n]$ the S functional for non-interacting electrons, we can write

$$A[n] = S_0[n] + S_H[n] + S_{xc}[n] - \int_{t_0}^{t_1} \int n(\mathbf{r},t) v_{ext}(\mathbf{r},t) dt d\mathbf{r} \tag{1.13}$$

where

$$S_H[n] = -\frac{1}{2} \int_{t_0}^{t_1} \int \int \frac{n(\mathbf{r},t) n(\mathbf{r}',t)}{|\mathbf{r}-\mathbf{r}'|} dt d\mathbf{r} d\mathbf{r}' \tag{1.14}$$

and S_{xc}, analogously to ground-state DFT, contains all the missing contributions to the functional $A[n]$. The stationary action principle leads to the equation

$$\frac{\delta S_0[n]}{\delta n(\mathbf{r},t)} - v_{KS}(\mathbf{r},t) = 0, \tag{1.15}$$

where

$$\begin{aligned} v_{KS}(\mathbf{r},t) &= v_H(\mathbf{r},t) + v_{xc}(\mathbf{r},t) + v_{ext}(\mathbf{r},t) & (1.16)\\ &= \int \frac{n(\mathbf{r}',t)}{|\mathbf{r}-\mathbf{r}'|} d\mathbf{r}' - \frac{\delta A_{xc}[n]}{\delta n(\mathbf{r},t)} + v_{ext}(\mathbf{r},t). & (1.17) \end{aligned}$$

Eq. (1.15) is precisely the Euler equation of a system of independent electrons moving in a time-dependent potential equal to $v_{KS}(\mathbf{r},t)$. Therefore, the exact density of the many-body system can be obtained from the set of fictitious one-particle time-dependent Schrödinger equations:

$$i\frac{\partial}{\partial t}\phi_i(\mathbf{r},t) = \left[-\frac{1}{2}\nabla^2 + v_{KS}(\mathbf{r},t)\right] \phi_i(\mathbf{r},t), \tag{1.18}$$

called time-dependent Kohn-Sham (TDKS) equations. From the orbitals ϕ_i the density can be build simply through the relation

$$n(\mathbf{r},t) = \sum_i^{N_v} \phi_i^*(\mathbf{r},t)\phi_i(\mathbf{r},t), \tag{1.19}$$

where the sum is over the occupied states. In the following sections we will analyze suitable approximations for v_{xc} and practical schemes to solve the TDDFT problem.

1.4 Adiabatic approximation

As ground-state DFT, the TDKS equations (1.18) require a suitable approximation for the xc potential in order to be applied in practice. The exact v_{xc} depends

non-locally on the density both in the spatial and in the time variables (memory dependence). Fortunately, by disregarding memory dependence, we obtain an approximation which is not too bad and that has been successfully applied in many cases. This approach, called the adiabatic exchange-correlation approximation (AXCA), can be written formally as

$$v_{xc}^{adia}[n](\mathbf{r},t) = v_{xc}^{GS}[n(t)](\mathbf{r}), \tag{1.20}$$

where v_{xc}^{GS} is the ground-state xc functional calculated at the instantaneous density, $n(t)$. Each ground-state functional such as LDA, GGA or hybrid can yield a corresponding adiabatic approximation. In the limit of an external potential that varies slowly in time, the AXCA becomes exact if the true xc ground-state functional is known. In practice the results are also affected by the faults of the ground-state approximations, such as the lack of spatial non-locality of LDA or GGA. Nevertheless, despite the crudeness of AXCA, optical spectra calculated within this approach are sometimes as accurate as the results of more demanding many-body approaches [5].

There are several known failures of the AXCA, due to either lack of memory or spatial non-locality. Among them we mention the optical properties of solids and long conjugated molecules, double excitations, and charge-transfer excitations. These faults of AXCA and the attempts to solve them are reviewed in [41].

All applications of TDDFT in this thesis will use AXCA.

1.5 Linear response theory and optical properties

The majority of applications of TDDFT concerns the calculation of optical absorption spectra in the linear regime using the dipole approximation. The results of such calculations can be compared with the findings of standard spectroscopic experiments, where the external perturbing field is weak. In this section we will summarize the general results of linear response theory, with emphasis on its application to optical absorption spectra. Linear response theory is a straightforward consequence of the time-dependent Schrödinger equation in a perturbative treatment. For convenience, the equations will be considered in the frequency representation, obtained by Fourier transforming time-dependent quantities.

Given a many-particle system, the purpose of linear response theory is to study the variation of a given physical observable due to the application of a weak external perturbation. As it is usual in quantum mechanics, both the observable and the perturbation are represented by Hermitian operators. The fundamental quantity in time-dependent linear response theory is the generalized susceptibility which in the frequency domain (Lehmann representation) can be written [63]

$$\begin{aligned}\chi(\mathbf{r},\mathbf{r}',\omega) &= \sum_n \left[\frac{\langle\Psi_0|\hat{\psi}^\dagger(\mathbf{r})\hat{\psi}(\mathbf{r})|\Psi_n\rangle\langle\Psi_n|\hat{\psi}^\dagger(\mathbf{r}')\hat{\psi}(\mathbf{r}')|\Psi_0\rangle}{\omega-(E_n-E_0)+i\eta} \right. \\ &\left. - \frac{\langle\Psi_0|\hat{\psi}^\dagger(\mathbf{r}')\hat{\psi}(\mathbf{r}')|\Psi_n\rangle\langle\Psi_n|\hat{\psi}^\dagger(\mathbf{r})\hat{\psi}(\mathbf{r})|\Psi_0\rangle}{\omega+(E_n-E_0)+i\eta} \right], \quad (1.21)\end{aligned}$$

where η is an infinitesimal positive number, Ψ_0 and Ψ_n are respectively the ground-state and excited-state wave functions corresponding to the energies E_0 and E_n, and $\hat{\psi}^\dagger(\mathbf{r})$ and $\hat{\psi}(\mathbf{r})$ are field operators. The operator $\hat{\psi}^\dagger(\mathbf{r})\hat{\psi}(\mathbf{r})$ is the second-quantized version of the density operator $\hat{n}(\mathbf{r}) = \sum_{i=1}^{N}\delta(\mathbf{r}-\mathbf{r_i})$, where N is the number of electrons. The poles of Eq. (1.21) correspond to the excitation energies of the system. Using Eq. (1.21) the Fourier transform of the response of the expectation value of a local operator, $\hat{A}$, to a local time-dependent perturbation $v'_{ext}(\mathbf{r},t)$ reads:

$$A'(\omega) = \int A(\mathbf{r})\chi(\mathbf{r},\mathbf{r}',\omega)v'_{ext}(\mathbf{r}',\omega)d\mathbf{r}d\mathbf{r}'. \quad (1.22)$$

In case of an independent-particle system Ψ_0 and Ψ_n become Slater determinants of single-particle orbitals, $\phi_i(\mathbf{r})$, corresponding to the energies ε_i and Eq. (1.21) can be written as

$$\chi(\mathbf{r},\mathbf{r}',\omega) = \sum_{ij}(n_j-n_i)\frac{\phi_j^*(\mathbf{r})\phi_i(\mathbf{r})\phi_i^*(\mathbf{r}')\phi_j(\mathbf{r}')}{\varepsilon_j-\varepsilon_i+\omega+i\eta}, \quad (1.23)$$

where n_j and n_i are the occupation numbers; this equation is particularly useful in TDDFT since it is used to calculate the KS susceptibility.
A particularly important specific linear response function is polarizability

$$\alpha_{ij}(\omega) = \int r_i\chi(\mathbf{r},\mathbf{r}',\omega)r'_j d\mathbf{r}d\mathbf{r}', \quad (1.24)$$

where r_i and r'_j are the components of the position operators $\mathbf{r}$ and $\mathbf{r}'$ in the first-quantized form. If we indicate with $\mathbf{d}'(\omega)$ the linear response of the dipole to the

external perturbation $v'_{ext}(\mathbf{r},\omega) = -\mathbf{E}(\omega)\cdot\mathbf{r}$ (where $\mathbf{E}(\omega)$ is a weak electric field), we can write polarizability as

$$\alpha_{ij}(\omega) = \frac{d'_i(\omega)}{E_j(\omega)}, \tag{1.25}$$

namely the response tensor of the dipole to an external electric field. Usually, in the case of unpolarized radiation, the mean polarizability is written in the form

$$\bar{\alpha}(\omega) = \frac{1}{3}Tr\alpha(\omega) = \sum_n \frac{f_n}{(E_n - E_0)^2 - \omega^2}, \tag{1.26}$$

where we defined the spectroscopic oscillator strengths

$$f_n = \frac{2}{3}(E_n - E_0)(|\langle\Psi_0|\hat{x}|\Psi_n\rangle|^2 + |\langle\Psi_0|\hat{y}|\Psi_n\rangle|^2 + |\langle\Psi_0|\hat{z}|\Psi_n\rangle|^2), \tag{1.27}$$

and $\hat{x}$, $\hat{y}$ and $\hat{z}$ are the components of the position operator. Eq. (1.26) is a straightforward consequence of Eq. (1.21) and of Eq. (1.24). Polarizability is particularly important since it is strictly related to the absorption of electromagnetic radiation in the dipole approximation. Indeed for a molecular system we can write the absorption coefficient as

$$I(\omega) \propto \omega \mathrm{Im}\,(\bar{\alpha}(\omega)). \tag{1.28}$$

This relation can be obtained in the context of the semi-classical theory of the interaction radiation-matter using the dipole approximation and *Fermi's golden rule*. Since this result has been used extensively in the thesis we will sketch here the demonstration. First of all we remind that the absorption coefficient I is defined by the relation $F(z) = F_0 e^{-Iz}$, where F indicates the intensity of an electromagnetic beam propagating along z. We also remind that the density of the energy of radiation is given by $\rho = \frac{E^2}{8\pi}$, where E is the norm of the electric field associated with the wave. The intensity F is provided by the product $c\rho$ where c is the speed of light. Using these relations, the energy per unit of time which is provided to the system under investigation by the light beam can be written as

$$\frac{dU}{dt} = c\frac{dU}{dz} = \frac{Vc}{8\pi}\frac{dE^2}{dz} = -\frac{Vc}{8\pi}IE^2, \tag{1.29}$$

where V denotes the volume. This equation can be inverted to obtain

$$I = -\frac{8\pi}{VcE^2}\frac{dU}{dt}. \tag{1.30}$$

In order to establish a connection with microscopic theory we rewrite Eq. (1.29) as

$$\frac{dU}{dt} = \sum_{if} \omega_{fi} W_{if}, \tag{1.31}$$

where i and f indicate occupied and empty energy levels, ω_{fi} is their difference in energy, and W_{if} is the transition probability per unit of time between levels i and f. To go further we have now to evaluate W_{if} using quantum mechanics. We will consider the simple case of a single electron subject to an external potential $v_{ext}(\mathbf{r})$ and to electromagnetic radiation. The Hamiltonian for this system can be expressed as

$$H = \frac{1}{2}(-i\nabla - \frac{\mathbf{A}}{c})^2 + v_{ext}(\mathbf{r}) \tag{1.32}$$

where $\mathbf{A}$ is the vector potential associated with the electromagnetic wave. Using the Coulomb gauge $\nabla \cdot \mathbf{A} = 0$ and discarding the quadratic term in the vector potential, Eq. (1.32) can be simplified as

$$H = -\frac{1}{2}\nabla^2 + v_{ext}(\mathbf{r}) + \frac{i}{c}\mathbf{A} \cdot \nabla, \tag{1.33}$$

where the last term of the Hamiltonian can be treated perturbatively. For an electromagnetic wave propagating along z, the vector potential can be chosen to be

$$\mathbf{A}(z,t) = \mathbf{A}_0 e^{i(kz-\omega t)}, \tag{1.34}$$

where k is the wave number and ω is the frequency. In general, if the wavelength λ of the radiation is large if compared with the dimension of the system under investigation, the vector potential can be expanded in powers of $kz = \frac{2\pi}{\lambda}z$:

$$\mathbf{A}(z,t) = \mathbf{A}_0 e^{-i\omega t}[1 + ikz - \frac{1}{2}(kz)^2 + \ldots]. \tag{1.35}$$

By limiting the expansion to the first term, namely by discarding the dependence on the position, we obtain the dipole approximation. Using Fermi's golden rule, the transition probability per unit of time between two levels i (occupied) and f (unoccupied) is given by

$$W_{if} = \frac{2\pi}{c^2}[\mathbf{A}_0 \cdot \langle \Psi_f | \nabla | \Psi_i \rangle]^2 \delta(\omega_{fi} - \omega). \tag{1.36}$$

Through the identity $[\mathbf{r}, H] = \nabla$, the term $\langle \Psi_f | \nabla | \Psi_i \rangle$ can be expressed as

$$\langle \Psi_f | \nabla | \Psi_i \rangle = -\omega_{fi} \langle \Psi_f | \mathbf{r} | \Psi_i \rangle, \tag{1.37}$$

and Eq. (1.36) can be finally written as

$$W_{if} = 2\pi [\mathbf{E}_0 \cdot \langle \Psi_f | \mathbf{r} | \Psi_i \rangle]^2 \delta(\omega_{fi} - \omega), \tag{1.38}$$

where we used the relation $\mathbf{E}_0 = \frac{i\omega_{fi}}{c}\mathbf{A}_0$. Now W_{if} is ready to be inserted in Eq. (1.31) to obtain the absorption coefficient through Eq. (1.30). It is now straightforward to note the equivalence of Eq. (1.28) and Eq. (1.30).

1.6 Linear response TDDFT and Dyson-like equation

According to Eq. (1.22), the perturbation v'_{ext} introduces a first-order change in the electronic density that can be expressed for an interacting system as

$$n'(\mathbf{r}, \omega) = \int \chi(\mathbf{r}, \mathbf{r}', \omega) v'_{ext}(\mathbf{r}', \omega) d\mathbf{r}', \tag{1.39}$$

where χ is the generalized susceptibility defined in Eq. (1.21). By construction, the non interacting Kohn-Sham equations (1.18) have the same time-dependent density as the many-body problem. For this reason, the response of the density $n'(\mathbf{r}, \omega)$ is also the same. In this case the equations are a bit more subtle, since the effective potential also depends on the internal variables. Indeed the response of the density can be written as

$$n'(\mathbf{r}, \omega) = \int \chi_{KS}(\mathbf{r}, \mathbf{r}', \omega) v'_{KS}(\mathbf{r}', \omega) d\mathbf{r}', \tag{1.40}$$

where

$$v'_{KS}(\mathbf{r}, \omega) = v'_{ext}(\mathbf{r}, \omega) + v'_H(\mathbf{r}, \omega) + v'_{xc}(\mathbf{r}, \omega), \tag{1.41}$$

and χ_{KS} is the KS susceptibility

$$\chi_{KS}(\mathbf{r}, \mathbf{r}', \omega) = \sum_{ij} (n_j - n_i) \frac{\phi_j^*(\mathbf{r}) \phi_i(\mathbf{r}) \phi_i^*(\mathbf{r}') \phi_j(\mathbf{r}')}{\varepsilon_j - \varepsilon_i + \omega + i\eta}, \tag{1.42}$$

with ϕ_i and ϕ_j denoting the ground-state KS orbitals corresponding to the eigenvalues ε_i and ε_j. It is important to notice that, if i an j are both occupied or empty levels, the corresponding contribution to χ vanishes. In Eq. (1.41) we have introduced the first-order response of the Hartree+xc correlation potential induced by the application of v'_{ext}

$$v'_{Hxc}(\mathbf{r},\omega) = v'_H(\mathbf{r},\omega) + v'_{xc}(\mathbf{r},\omega) = \int \kappa(\mathbf{r},\mathbf{r}',\omega) n'(\mathbf{r}',\omega) d\mathbf{r}'; \tag{1.43}$$

the kernel κ is defined by

$$\kappa(\mathbf{r},\mathbf{r}',\omega) = \frac{1}{|\mathbf{r}-\mathbf{r}'|} + \left.\frac{\delta v_{xc}(\mathbf{r},\omega)}{\delta n(\mathbf{r}',\omega)}\right|_{n=n_0} \tag{1.44}$$

where the second term is a functional of ground-state density only. In the AXCA Eq. (1.44) does not depend explicitly on frequency because the xc contribution to the kernel is local in time:

$$f_{xc}^{adia}(\mathbf{r},\mathbf{r}',t-t') = \left.\frac{\delta v_{xc}(\mathbf{r})}{\delta n(\mathbf{r}')}\right|_{n=n_0} \delta(t-t'). \tag{1.45}$$

By equating the density response in Eq. (1.39) and Eq. (1.40) and by using Eq. (1.43), we obtain the Dyson-like equation of TDDFT linear response:

$$\chi(\mathbf{r},\mathbf{r}',\omega) = \chi_{KS}(\mathbf{r},\mathbf{r}',\omega) + \int\int \chi_{KS}(\mathbf{r},\mathbf{r}_1,\omega)\kappa(\mathbf{r}_1,\mathbf{r}_2,\omega)\chi(\mathbf{r}_2,\mathbf{r}',\omega) d\mathbf{r}_1 d\mathbf{r}_2. \tag{1.46}$$

The poles of the response function χ are excitation energies of the interacting system and the residues are the corresponding oscillator strength. The kernel κ is responsible for the corrections to the non interacting KS susceptibility (1.42). Indeed if we set $\kappa = 0$ we obtain exactly $\chi = \chi_{KS}$. The optical spectra can be obtained from the Dyson-like equation through Eq. (1.24).

The practical solution of Eq. (1.46) is an expensive operation both from a computational and a memory-requirement points of view. The first expensive task is the calculation of the empty states of the ground-state KS Hamiltonian, an operation which scales as the third power of the dimension of the basis set; in practice a smaller number of states is calculated thus limiting the applicability to a lower energy range. The next step consists in constructing the independent-particle susceptibility χ_{KS}; in order to perform this operation in real space or

reciprocal space, we have a computational effort of the order $N_v N_c N_{grid}^2$ (N_v and N_c are the number of occupied states and of empty states respectively and N_{grid} is the dimension of the grid) and a storage amount of N_{grid}^2 complex numbers. At this point we are ready to solve the Dyson-like equation, which requires dense-matrix multiplications and inversions, whose cost is proportional to N_{grid}^3. This procedure, apart from the calculation of empty states, has to be repeated for each frequency. In practice, because of its unfavorable scaling, this approach is feasible only for systems consisting of a small number of atoms. As we will see in the next sections and in Chapter 2, there are more efficient ways to cope with the problem of optical properties.

1.7 Casida's equations

For frequency-independent kernels, Casida has reformulated the calculation of the poles (namely the transition energies) of the response function χ into a generalized Hermitian eigenvalue problem [49]. This approach is the most widespread in the quantum chemistry community and is implemented in many ab initio codes. It is particularly suitable to calculate optical properties, although it is not possible to access broad energy ranges.

The starting point to derive Casida's equations is Eq. (1.40) where v'_{Hxc} in turn depends linearly upon the response of the density through Eq. (1.43). By explicitly substituting the KS susceptibility (1.42) in Eq. (1.40), we notice that the factorization allows for a direct integration of the product of the response function and of the first order change in the potential. The induced density change can then be written as

$$n'(\mathbf{r},\omega) = \sum_{ij} P'_{ij} \phi_j^*(\mathbf{r}) \phi_i(\mathbf{r}), \tag{1.47}$$

in which the expansion coefficients are given by

$$P'_{ij}(\omega) = \frac{n_j - n_i}{\varepsilon_j - \varepsilon_i + \omega + i\eta} \int \phi_i^*(\mathbf{r}) v'_{KS}(\mathbf{r},\omega) \phi_j(\mathbf{r}) d\mathbf{r}. \tag{1.48}$$

These coefficients are different from zero only if they connect virtual states with occupied states and vice versa. By inserting explicitly n' in the form of Eq. (1.47) in Eq. (1.43) and by using this last equation to evaluate Eq. (1.48), we obtain the

linear system

$$\sum_{kl}\left[\frac{\omega-(\varepsilon_k-\varepsilon_l)}{n_j-n_i}\delta_{ik}\delta_{jl}-k_{ij,kl}\right]P'_{kl}(\omega)=\int\phi_i^*(\mathbf{r})v'_{ext}(\mathbf{r},\omega)\phi_j(\mathbf{r})d\mathbf{r}, \quad (1.49)$$

where

$$k_{ij,kl}(\omega)=\int\int\phi_i^*(\mathbf{r})\phi_j(\mathbf{r})\kappa(\mathbf{r},\mathbf{r}',\omega)\phi_k^*(\mathbf{r}')\phi_l(\mathbf{r}') \quad (1.50)$$

is the coupling matrix and $\kappa(\mathbf{r},\mathbf{r}',\omega)$ is the exchange-correlation kernel given by Eq. (1.44). With some more algebra and by setting $v'_{ext}=0$, Eq. (1.49) can be written in the final form of Casida's equations

$$\hat{\Omega}F_I=\omega_I F_I, \quad (1.51)$$

where

$$\Omega_{ij,kl}=(\varepsilon_l-\varepsilon_k)^2\delta_{ik}\delta_{jl}+2\sqrt{(n_i-n_j)(\varepsilon_j-\varepsilon_i)}\kappa_{ij,kl}\sqrt{(n_k-n_l)(\varepsilon_l-\varepsilon_k)} \quad (1.52)$$

is a Hermitian matrix. The eigenvalues of Eq. (1.51) provide the excitation energies of the system; the eigenvectors, instead, can be used to obtain the spectroscopic oscillator strengths and to assign the symmetry of each transition.

First of all, in order to solve Casida's equations, it is necessary to diagonalize the ground-state Hamiltonian in order to obtain all (or at least many of) the empty KS states. This operation has an unfavorable scaling, which makes this approach not particularly appropriate for large basis sets, such as plane-waves. The most straightforward (and naive) way to proceed is to calculate the N_vN_c dimensional matrix $\Omega_{ij,kl}$ explicitly and to store it. The most computational demanding task is to calculate the coupling matrix in Eq. (1.50); indeed, if we suppose to calculate it in real space, the computational cost amounts to $N_{grid}^2N_v^2N_c^2$, but it usually decreases for the xc part since this term is local (at least in ALDA). This rough estimation shows a really unfavorable scaling as the 6th power of the system dimension. Once the matrix is constructed we have to diagonalize it and this requires a cost that scales as $N_v^3N_c^3$. In practice this is never done. It is possible to take advantage of iterative techniques [64] that do not require the explicit calculation and storage of the full matrix Ω. Indeed the coupling matrix can be evaluated using techniques, which are already well established for ground-state calculations, such as the auxiliary function expansion method for localized basis

sets [65] or fast Fourier transforms in plane-wave implementations [Appendix A]. In this scheme the computational cost is significantly reduced. The real drawback of this approach is that iterative techniques allow for the calculation of only a limited number of the lowest eigenvalues. Furthermore serious problems can arise when particularly large systems have to be treated. Indeed, by increasing the size of the system, the density of transitions in a given energy range increases as well.

1.8 Real-time propagation

In this section we will present a further practical method to solve TDDFT equations. As a starting point for our calculation, we can choose the time-dependent KS equations (1.18) and directly integrate them. Besides displaying better numerical properties than the previous methods, the real-time propagation of KS equations also allows to account for non-linear effects. Starting from a system which is initially in its ground-state at $t = 0$, we can calculate the density at a time $t = t'$, $n(\mathbf{r}, t')$, by propagating the occupied ground-state KS orbitals

$$\phi_v(\mathbf{r}, t') = \hat{U}(t', 0)\phi_v(\mathbf{r}), \tag{1.53}$$

where $\hat{U}$ is the time evolution operator

$$\hat{U}(t', 0) = \hat{\mathcal{T}} \exp\{-i \int_0^{t'} \hat{H}(\tau) d\tau\}, \tag{1.54}$$

and $\hat{\mathcal{T}}$ is the time ordering operator. Within this approach the density at a time t' can be written as $n(\mathbf{r}, t') = \sum_v |\phi_v(\mathbf{r}, t')|^2$. For practical purposes the propagation problem is performed by splitting the time interval from $t = 0$ to $t = t'$ in small steps δt using the well-known property $\hat{U}(t_2, t_1) = \hat{U}(t_2, t_3)\hat{U}(t_3, t_1)$:

$$\phi_v(\mathbf{r}, t + \delta t) = \hat{U}(t + \delta t, t)\phi_v(\mathbf{r}, t). \tag{1.55}$$

In real calculations it is necessary to choose particularly suitable approximations for the time evolution operator $\hat{U}(t + \delta t, t)$ both from the point of view of computational cost and numerical accuracy. A review of the many different practical methods is given in [66]. In general these approximations should reproduce in a sufficiently accurate way the exact properties of $\hat{U}$, such as unitarity, which is

essential to ensure the conservation of the total charge during the propagation. A particularly simple approach is the midpoint rule, which consists in approximating the propagator by the exponential of the Hamiltonian calculated at time $t + \delta t/2$, namely

$$\hat{U}(t + \delta t, t) = \exp\{-i\hat{H}(t + \frac{\delta t}{2})\delta t\} \tag{1.56}$$

where $\hat{H}(t + \frac{\delta t}{2})$ is obtained self-consistently using a predictor corrector method [18]. The exponential, in order to be evaluated, is expanded in Taylor series to a given order and Eq. (1.55) becomes

$$\phi_v(\mathbf{r}, t + \delta t) = [1 - i\hat{H}(t + \frac{\delta t}{2})\delta t - \frac{1}{2}\hat{H}^2(t + \frac{\delta t}{2})\delta t^2 + \ldots]\phi_v(\mathbf{r}, t); \tag{1.57}$$

this equation shows that the calculation can be carried out by repeated applications of the Hamiltonian $\hat{H}$ to an orbital. This same operation is required for iterative ground-state DFT calculations and thus TDDFT can take advantage of techniques already developed for standard static DFT (see appendix A for the case of plane-wave basis set).

In the specific case of the calculation of linear response spectra, an external time-dependent potential $v'_{ext}(\mathbf{r}, t) = -\bar{E}\delta(t)\mathbf{r}$ is introduced in Eq. (1.18), where $\bar{E}$ is a parameter which has to be small enough to ensure the linear response regime. From a physical point of view we are basically applying an external homogeneous electric field $\bar{E}$ to the system at the initial time $t = 0$. This perturbation excites all the frequencies with the same weight. Soon after $t = 0$ we turn off this perturbation and let the system evolve. It is important to note that the Hamiltonian in Eq. (1.18) is still time-dependent for $t > 0$, since it depends on the density $n(\mathbf{r}, t)$ which changes in time. We can now calculate the polarizability $\alpha_{ij}(\omega) = d'_i(\omega)/E_j(\omega)$ by Fourier transforming the time-dependent dipole

$$d'_i(t) = \int r_i n'(\mathbf{r}, t) d\mathbf{r} = \sum_v \langle\phi_v(t)|r_i|\phi_v(t)\rangle \tag{1.58}$$

to obtain

$$d'_i(\omega) = \int_0^\infty e^{i\omega t - \eta t} d_i(t) dt \tag{1.59}$$

and dividing it by $E_j(\omega) = \bar{E}$. In order to make the integral converge, in Eq. (1.59) a damping factor $e^{-\eta t}$ has been introduced; the effect of this term is to broaden the final spectrum.

The first advantage of this method is that it is sufficient to calculate the occupied states of the ground-state KS Hamiltonian and this is essential when a large basis set is used. The second important point is that it is possible to calculate the response function in a wide range of frequencies with a single propagation. In practice there is a connection between the time step used and the maximum frequency that we can calculate, namely $\omega_{max} = 1/\delta t_{max}$. The choice of the time step is mainly determined by numerical stability problems.

The computational cost of this method is related to the implementation of the time propagation operator $\hat{U}$ and to the total number of steps necessary to reach the final result. As Eq. (1.57) shows for a specific case, each step of the evolution requires several applications (depending on the algorithm used) of the Hamiltonian to a number of orbitals equal to the number of occupied states; this is the same kind of operation required to solve the ground-state problem by using iterative techniques, such as Davidson [64] or to perform first-principles molecular dynamics [67]. For this reason the numerical scalability of this method is the same as the ground-state problem; the prefactor, instead, is less favorable, since the Hamiltonian has to be applied many more times at each iterative step and since the total number of steps is larger. Despite this relatively large prefactor, the properties of this method make it particularly suitable for applications to large systems.

Chapter 2

The Liouville-Lanczos approach

In this chapter we will introduce a new approach to solve TDDFT equations which is particularly suitable to calculate spectra of molecules or extended systems in a very large energy range and with a computational scaling equal to that of standard ground-state applications. The starting point is the linearization of TDDFT equations, which has already been considered in Chapter 1. In this chapter for our purposes we choose an elegant approach based on density matrices and super-operators. Within this formulation we are able to express the molecular polarizability (but also other response functions) as an off diagonal element of the resolvent of the Liouvillian super-operator. Through an explicit representation of density matrices borrowed from time-independent density functional perturbation theory we can avoid the calculation of KS empty states and we can evaluate the polarizability using a newly developed Lanczos algorithm. Finally, to prove its reliability, we proceed to test the new method against the benchmark case of benzene absorption spectrum.

2.1 Density matrix formulation of linear response TDDFT

In this section we will consider the linearization of TDKS equations in quite the same spirit as Chapter 1 but we will use a slightly different formalism. We start

from the quantum Liouville equation

$$i\frac{d\hat{\rho}(t)}{dt} = \left[\hat{H}_{KS}(t), \hat{\rho}(t)\right], \tag{2.1}$$

which rules the time evolution of the reduced one-electron KS density matrix $\hat{\rho}(t)$ whose kernel reads:

$$\rho(\mathbf{r}, \mathbf{r}', t) = \sum_{v=1}^{N_v} \phi_v(\mathbf{r}, t)\phi_v^*(\mathbf{r}', t), \tag{2.2}$$

where ϕ_v are the occupied KS orbitals. In Eq. (2.1) square brackets indicate a commutator and

$$\hat{H}_{KS}(t) = -\frac{1}{2}\nabla^2 + v_{ext}(\mathbf{r}, t) + v_{Hxc}(\mathbf{r}, t) \tag{2.3}$$

is the time-dependent KS Hamiltonian. In the above equation, as well as in the following, quantum-mechanical operators are denoted by a hat, " ˆ "; when no confusion can arise, local operators, such as one-electron potentials, $\hat{v}$, will be indicated by the diagonal of their real-space representation, $v(\mathbf{r})$, as in Eq. (2.3). For our purposes we could have started directly from TDKS equations (1.18) but we have chosen this formulation for its simplicity and elegance. Let us suppose now that the external potential $v_{ext}(\mathbf{r}, t)$ is composed by a time-independent part $v_{ext}^{GS}(\mathbf{r})$ (namely the ground-state external potential) plus a small time-dependent part $v'_{ext}(\mathbf{r}, t)$, which can be treated perturbatively. To solve the quantum Liouville equation let us set the initial condition $\hat{\rho}(0) = \hat{\rho}_0$, where $\hat{\rho}_0$ is the ground-state density matrix. Linearization of Eq. (2.1) with respect to the external perturbation leads to:

$$i\frac{d\hat{\rho}'(t)}{dt} = \left[\hat{H}_{KS}^{GS}, \hat{\rho}'(t)\right] + [\hat{v}'_{Hxc}(t), \hat{\rho}_0] + [\hat{v}'_{ext}(t), \hat{\rho}_0], \tag{2.4}$$

where $\hat{\rho}'(t)$ is the first order response of the density matrix, $\hat{H}_{KS}^{GS}$ is the time-independent ground-state Hamiltonian, $\hat{v}'$ is the perturbing external potential, and $\hat{v}'_{Hxc}$ is the time domain representation of Eq. (1.43):

$$v'_{Hxc}(\mathbf{r}, t) = \int \kappa(\mathbf{r}, \mathbf{r}', t - t')n'(\mathbf{r}', t')d\mathbf{r}'dt', \tag{2.5}$$

where $n'(\mathbf{r}, t) = \rho'(\mathbf{r}, \mathbf{r}, t)$. By inserting this expression into Eq. (2.4), one sees that the linearized Liouville equation can be cast into the form:

$$i\frac{d\hat{\rho}'(t)}{dt} = \mathcal{L} \cdot \hat{\rho}'(t) + [\hat{v}'_{ext}(t), \hat{\rho}_0], \tag{2.6}$$

where the action of the *Liouvillian super-operator*, $\mathcal{L}$, onto $\hat{\rho}'$, $\mathcal{L}\cdot\hat{\rho}'$, is defined as:

$$\mathcal{L}\cdot\hat{\rho}' = \left[\hat{H}_{KS}^{GS},\hat{\rho}'\right] + [\hat{v}'_{Hxc}[\hat{\rho}'](t),\hat{\rho}_0]\,, \tag{2.7}$$

where we have explicitly written the (linear) functional dependence of v'_{Hxc} on $\hat{\rho}'$. By Fourier analyzing Eq. (2.6) we obtain:

$$(\omega-\mathcal{L})\cdot\hat{\rho}'(\omega) = [\hat{v}'_{ext}(\omega),\hat{\rho}_0]\,. \tag{2.8}$$

In the absence of any external perturbation ($v'_{ext}(\mathbf{r},\omega)=0$), Eq. (2.8) becomes an eigenvalue equation for $\hat{\rho}'$, whose eigenpairs describe free oscillations of the system, *i.e.* excited states [49]. Eigenvalues correspond to excitation energies, whereas eigenvectors can be used to calculate transition oscillator strengths, and/or the response of system properties to external perturbations.

One is hardly interested in the response of the most general property of a system to the most general perturbation. When simulating the results of a specific spectroscopy experiment, in fact, one is usually interested in the response of a *specific* observable to a *specific* perturbation. The expectation value of any one-electron operator can be expressed as the trace of its product with the one-electron density matrix. As shown in Chapter 1, a particularly important response function is polarizability, namely the response of the dipole to an external electric field. In our formalism the frequency domain response of the dipole induced by the perturbing potential $v'_{ext}(\mathbf{r},\omega)$ can be expressed as

$$\mathbf{d}(\omega) = \mathrm{Tr}\left(\hat{\mathbf{r}}\hat{\rho}'(\omega)\right), \tag{2.9}$$

where $\hat{\mathbf{r}}$ is the position operator, and $\hat{\rho}'(\omega)$ is the solution to Eq. (2.8). If we write the perturbation explicitly in terms of an external homogeneous electric field

$$v'_{ext}(\mathbf{r},\omega) = -\mathbf{E}(\omega)\cdot\mathbf{r}. \tag{2.10}$$

the dipole given by Eq. (2.9) can be expressed as

$$d_i(\omega) = \sum_j \alpha_{ij}(\omega)E_j(\omega), \tag{2.11}$$

where the dynamical polarizability, $\alpha_{ij}(\omega)$, is defined by

$$\alpha_{ij}(\omega) = -\mathrm{Tr}\left(\hat{r}_i(\omega-\mathcal{L})^{-1}\cdot[\hat{r}_j,\hat{\rho}_0]\right). \tag{2.12}$$

Traces of products of operators can be seen as scalar products defined on the linear space of operators. Let $\hat{A}$ and $\hat{B}$ be two general one-electron operators. We define their *scalar product* as:

$$\left\langle \hat{A}|\hat{B}\right\rangle \equiv \mathrm{Tr}\left(\hat{A}^{\dagger}\hat{B}\right). \tag{2.13}$$

Eq. (2.12) can therefore be formally written as:

$$\alpha_{ij}(\omega) = -\left\langle \hat{r}_i|(\omega-\mathcal{L})^{-1}\cdot\hat{s}_j\right\rangle, \tag{2.14}$$

where

$$\hat{s}_j = [\hat{r}_j, \hat{\rho}_0] \tag{2.15}$$

is the commutator between the position operator and the unperturbed one-electron density matrix. The results obtained so far and embodied in Eq. (2.14) can be summarized by saying that *within TDDFT the dynamical polarizability can be expressed as an appropriate off-diagonal matrix element of the resolvent of the Liouvillian super-operator*. A similar conclusion was reached in Ref. [68] in the context of a localized basis set formalism. This statement can be extended in a straightforward way to the dynamic linear response of any observable to any local one-electron perturbation. It is worth noticing that the operators that enter the definition of the scalar product in Eq. (2.14) are orthogonal because $\hat{r}_i$ is Hermitian and $\hat{s}_j$ anti-Hermitian (being the commutator of two Hermitian operators), and the trace of the product of one Hermitian operator and one anti-Hermitian operator vanishes.

2.2 Explicit representation of density matrices

The calculation of polarizability using Eqs. (2.12) or (2.14) implies that we should be able to compute $(\omega-\mathcal{L})^{-1}\cdot[\hat{r}_j,\hat{\rho}_0]$, namely to solve a super-operator linear system. The latter task, in turn, requires an explicit representation for the density-matrix response, $\hat{\rho}'$, for its commutator with the unperturbed Hamiltonian, for local operators, such as $\hat{r}_j$ of $v'_{Hxc}(\mathbf{r})$, for their commutators with the unperturbed density matrix, as well as for the Liouvillian super-operator, or at least for its product with any relevant operators, $\hat{A}$, such as $\mathcal{L}\cdot\hat{A}$.

A link between the orbital and density-matrix representations of TDDFT can be obtained by linearizing the expression (2.2) for the time-dependent density

matrix:

$$\rho'(\mathbf{r},\mathbf{r}';t) = \sum_v \left[\phi_v(\mathbf{r})\phi'^*_v(\mathbf{r}',t) + \phi'_v(\mathbf{r},t)\phi^*_v(\mathbf{r}')\right], \tag{2.16}$$

whose Fourier transform reads:

$$\rho'(\mathbf{r},\mathbf{r}';\omega) = \sum_v \left[\phi_v(\mathbf{r})\phi'^*_v(\mathbf{r}',-\omega) + \phi'_v(\mathbf{r},\omega)\phi^*_v(\mathbf{r}')\right]. \tag{2.17}$$

Eq. (2.17) shows that $\rho'(\omega)$ is univocally determined by the two sets of orbital response functions, $\mathbf{x}' = \{\phi'_v(\mathbf{r},\omega)\}$ and $\mathbf{y}' = \{\phi'^*_v(\mathbf{r},-\omega)\}$. A set of a number of orbitals equal to the number of occupied states, such as $\mathbf{x}'$ or $\mathbf{y}'$, will be nicknamed a *batch* of orbitals. We have to note now that $\rho(\omega)$ is *not* Hermitian because the Fourier transform of a Hermitian operator is not Hermitian, unless the original operator is even with respect to time inversion. Because of the orthogonality between occupied and response orbitals ($\langle\phi_v|\phi'_{v'}\rangle = 0$), Eq. (2.16) implies that the matrix elements of $\hat{\rho}'$ between two unperturbed KS orbitals which are both occupied or both empty vanish ($\rho'_{vv'} = \rho'_{cc'} = 0$), as required by the idempotency of density matrices in DFT. As a consequence, in order to calculate the variation of the expectation values of a Hermitian operator, $\hat{A}$, such as in Eq. (2.9), one only needs to know and represent the occupied-empty (*vc*) and empty-occupied (*cv*) matrix elements of $\hat{A}$, A_{vc} and A_{cv}. In other terms, if we define $\hat{P} = \sum_v |\phi_v\rangle\langle\phi_v| \doteq \hat{\rho}_0$ and $\hat{Q} \doteq 1 - \hat{P}$ as the projectors onto the occupied- and empty-state manifolds, respectively, one has that:

$$\mathrm{Tr}(\hat{A}\hat{\rho}'(\omega)) = \mathrm{Tr}(\hat{A}'\hat{\rho}'(\omega)), \tag{2.18}$$

where $\hat{A}' = \hat{P}\hat{A}\hat{Q} + \hat{Q}\hat{A}\hat{P}$ is the vc-cv component of $\hat{A}$, which can be easily and conveniently represented in terms of batches of orbitals. To this end, let us define the orbitals:

$$a^x_v(\mathbf{r}) = \hat{Q}\hat{A}\phi_v(\mathbf{r}) = \sum_c \phi_c(\mathbf{r})A_{cv}, \tag{2.19}$$

$$a^y_v(\mathbf{r}) = \left(\hat{Q}\hat{A}^\dagger\phi_v(\mathbf{r})\right)^* = \sum_c \phi^*_c(\mathbf{r})A_{vc}. \tag{2.20}$$

This representation is commonly used for density matrices in standard time-independent density functional perturbation theory [52, 53] and it has already been

applied to TDDFT in [54]; this approach is particularly efficient from a computational point of view because, in order to build $a_v^x(\mathbf{r})$ and $a_v^y(\mathbf{r})$, the calculation of empty states is not required. From Eqs. (2.19) and (2.20) one has:

$$A_{cv} = \langle \phi_c | a_v^x \rangle, \tag{2.21}$$

$$A_{vc} = \langle \phi_c^* | a_v^y \rangle. \tag{2.22}$$

If Eqs. (2.21)) and (2.22) are used to represent density matrices instead of Eqs. (2.19) and (2.20) we obtain exactly Eq. (1.48) and, consequently, we can reconstruct Casida's formalism. Therefore our formalism is equivalent to Casida's equations but differs in the explicit representation of density matrices. For the sake of simplicity and with no remarkable loss of generality, from now on we will assume that the unperturbed system is time-reversal invariant, so that the unperturbed KS orbitals, ϕ_v and ϕ_c, can be assumed to be real. The two batches of orbitals $\mathbf{a}^x \equiv \{a_v^x(\mathbf{r})\}$ and $\mathbf{a}^y = \{a_v^y(\mathbf{r})\}$ will be named the *batch representation* of the $\hat{A}$ operator, and will be indicated with the notation $(\mathbf{a}^x, \mathbf{a}^y)$ or $(\{a_v^x\}, \{a_v^y\})$. Scalar products between operators (traces of operator products) can be easily expressed in terms of their batch representations. Let $(\{b_v^x\}, \{b_v^y\})$ be the batch representation of the operator $\hat{B}$. If either of the two operators, $\hat{A}$ or $\hat{B}$, has vanishing vv and cc components, one has:

$$\begin{aligned} \left\langle \hat{A} | \hat{B} \right\rangle &= \mathrm{Tr}\left(\hat{A}^\dagger B \right) \\ &= \sum_{cv} \left(A_{cv}^* B_{cv} + A_{vc}^* B_{vc} \right) \\ &= \sum_{v} \left(\langle a_v^x | b_v^x \rangle + \langle a_v^y | b_v^y \rangle \right). \end{aligned} \tag{2.23}$$

If $\hat{A}$ is Hermitian, its batch representation satisfies the relation: $\mathbf{a}^y(\mathbf{r}) = \mathbf{a}^x(\mathbf{r})^*$, whereas anti-Hermiticity would imply: $\mathbf{a}^y(\mathbf{r}) = -\mathbf{a}^x(\mathbf{r})^*$. Due to time-reversal invariance and the consequent reality of the unperturbed KS orbitals, the batch representation of a real (imaginary) operator is real (imaginary).

In order to solve the super-operator linear system, Eq. (2.8), using the batch representation, one needs to work out the batch representation of $v'_{Hxc}(\mathbf{r},\omega)$ as a functional of ρ', as well as of the various commutators appearing therein. The

charge-density response to an external perturbation reads:

$$\begin{aligned} n'(\mathbf{r}) &= \sum_v \phi_v(\mathbf{r})\big(\phi'_v(\mathbf{r},\omega) + \phi'^*_v(\mathbf{r},-\omega)\big) \\ &= \sum_v \phi_v(\mathbf{r})\big(x'_v(\mathbf{r}) + y'_v(\mathbf{r})\big), \end{aligned} \tag{2.24}$$

where $(\{x'_v\},\{y'_v\})$ is the batch representation of the density-matrix response, ρ'. The Hartree-plus-xc potential response is:

$$v'_{Hxc}[\rho'](\mathbf{r}) = \int \kappa(\mathbf{r},\mathbf{r}')n'(\mathbf{r}')d\mathbf{r}' = \sum_v \int \kappa(\mathbf{r},\mathbf{r}')\phi_v(\mathbf{r}')\big(x'_v(\mathbf{r}') + y'_v(\mathbf{r}')\big)d\mathbf{r}'. \tag{2.25}$$

By using Eqs. (2.19) and (2.20) the batch representation of the Hartree-plus-xc potential response reads therefore

$$\begin{aligned} {v'}^x_{Hxc,v}(\mathbf{r}) &= \hat{Q}\sum_{v'}\int \phi_v(\mathbf{r})\kappa(\mathbf{r},\mathbf{r}')\phi_{v'}(\mathbf{r}')\big(x'_{v'}(\mathbf{r}') + y'_{v'}(\mathbf{r}')\big)d\mathbf{r}' \\ &\doteq \hat{Q}\sum_{v'}\int K_{vv'}(\mathbf{r},\mathbf{r}')\big(x'_{v'}(\mathbf{r}') + y'_{v'}(\mathbf{r}')\big)d\mathbf{r}' \qquad (2.26) \\ {v'}^y_{Hxc,v}(\mathbf{r}) &= {v'}^x_{Hxc,v}(\mathbf{r}), \qquad (2.27) \end{aligned}$$

where:

$$K_{vv'}(\mathbf{r},\mathbf{r}') = k(\mathbf{r},\mathbf{r}')\phi_v(\mathbf{r})\phi_{v'}(\mathbf{r}'). \tag{2.28}$$

Let $(\{{v'}^x_v\},\{{v'}^y_v\})$ be the batch representation of a local operator, $v'(\mathbf{r})$. The batch representation of the commutator between v' and the unperturbed density matrix, $v'' = [\hat{v}',\hat{\rho}_0]$, reads:

$$\begin{aligned} {v''}^x_v(\mathbf{r}) &= \hat{Q}[\hat{v}',\hat{\rho}_0]\phi_v(\mathbf{r}) \\ &= {v'}^x_v(\mathbf{r}) \qquad (2.29) \\ {v''}^y_v(\mathbf{r}) &= -{v''}^x_v(\mathbf{r}). \qquad (2.30) \end{aligned}$$

The batch representation of the commutator between the unperturbed Hamiltonian and the density-matrix response, $\rho'' = [\hat{H}^{GS}_{KS},\hat{\rho}']$, reads:

$$\begin{aligned} x''_v(\mathbf{r}) &= \hat{Q}[\hat{H}^{GS}_{KS},\hat{\rho}']\phi_v(\mathbf{r}) \\ &= (\hat{H}^{GS}_{KS} - \epsilon_v)x'_v(\mathbf{r}) \qquad (2.31) \\ y''_v(\mathbf{r}) &= -(\hat{H}^{GS}_{KS} - \epsilon_v)y'_v(\mathbf{r}). \qquad (2.32) \end{aligned}$$

The batch representation of the action of the Liouvillian on the density-matrix response appearing in Eq. (2.8) reads:

$$\mathcal{L}\begin{pmatrix} \mathbf{x}' \\ \mathbf{y}' \end{pmatrix} = \begin{pmatrix} \mathcal{D}+\mathcal{K} & \mathcal{K} \\ -\mathcal{K} & -\mathcal{D}-\mathcal{K} \end{pmatrix}\begin{pmatrix} \mathbf{x}' \\ \mathbf{y}' \end{pmatrix}, \tag{2.33}$$

where the action of the $\mathcal{D}$ and $\mathcal{K}$ super-operators on batches of orbitals is defined as:

$$\mathcal{D}\{x_v(\mathbf{r})\} = \{(\hat{H}^{GS}_{KS}-\epsilon_v)x_v(\mathbf{r})\} \tag{2.34}$$

$$\mathcal{K}\{x_v(\mathbf{r})\} = \left\{\hat{Q}\sum_{v'}\int K_{vv'}(\mathbf{r},\mathbf{r}')x_{v'}(\mathbf{r}')d\mathbf{r}'\right\}. \tag{2.35}$$

Note that, according to Eqs. (2.33), (2.34), and (2.35), the calculation of the product of the Liouvillian with a general one-electron operator in the batch representation only requires operating on a number of one-electron orbitals equal to the number of occupied KS states (number of electrons), without the need to calculate any empty states. In particular, the calculation of Eq. (2.35) is best performed by first calculating the Hxc potential generated by the fictitious charge density $\bar{n}(\mathbf{r}) = \sum_v x_v(\mathbf{r})\phi_v(\mathbf{r})$, and then by applying it to each unperturbed occupied KS orbital, $\phi_v(\mathbf{r})$. The projection of the resulting orbitals onto the empty-state manifold implied by the multiplication with $\hat{Q}$ is easily performed using the identity: $\hat{Q} = 1 - \sum_v |\phi_v\rangle\langle\phi_v|$.

It is convenient to perform a 45° rotation in the space of batches and define:

$$q_v(\mathbf{r}) = \frac{1}{2}\big(x_v(\mathbf{r})+y_v(\mathbf{r})\big) \tag{2.36}$$

$$p_v(\mathbf{r}) = \frac{1}{2}\big(x_v(\mathbf{r})-y_v(\mathbf{r})\big). \tag{2.37}$$

Eqs. (2.36) and (2.37) define the *standard batch representation* (SBR) of the density-matrix response. The SBR of the response charge density is:

$$n'(\mathbf{r},\omega) = 2\sum_v \phi_v(\mathbf{r})q_v(\mathbf{r},\omega) \tag{2.38}$$

The SBR of a general one-electron operator is defined in a similar way. In particular, the SBR of a real Hermitian operator has zero p component, whereas the SBR of the commutator of such an operator with the unperturbed density matrix

has zero q component. The standard batch representation of the TDDFT Liouville equation, Eq. (2.8), reads:

$$(\omega - \mathcal{L}) \begin{pmatrix} \mathbf{q}' \\ \mathbf{p}' \end{pmatrix} = \begin{pmatrix} \omega & -\mathcal{D} \\ -\mathcal{D} - 2\mathcal{K} & \omega \end{pmatrix} \begin{pmatrix} \mathbf{q}' \\ \mathbf{p}' \end{pmatrix} = \begin{pmatrix} 0 \\ \{\hat{Q} v'_{ext}(\mathbf{r}) \phi_v(\mathbf{r})\} \end{pmatrix}. \tag{2.39}$$

If we set v'_{ext} in this equation we obtain an eigenvalue equation whose eigenvalues are the excitations energies of the system.

It is now straightforward to write explicitly the SBR of polarizability (2.14):

$$\alpha_{ij}(\omega) = -\left\langle (\{\hat{Q} r_i \phi_v\}, 0) | (\omega - \mathcal{L})^{-1} \cdot (0, \{\hat{Q} r_j \phi_v\}) \right\rangle, \tag{2.40}$$

where we used Eq. (2.39) with $v'_{ext} = -E_j(\omega) r_j$ and Eq. (2.23), where in this specific case $a_v^x(\mathbf{r}) = a_v^y(\mathbf{r}) = \hat{Q} r_i \phi_v(\mathbf{r})$. It is evident that the left batch vector $(\{\hat{Q} r_i \phi_v\}, 0)$ and the right one $(0, \{\hat{Q} r_j \phi_v\})$ are orthogonal.

2.3 Linear response functions from Lanczos recursion chains

According to Eq. (2.40), the polarizability can be expressed as an appropriate off-diagonal matrix element of the resolvent of the non-Hermitian Liouvillian (super-) operator between two orthogonal vectors. The standard way to calculate such a matrix element is to solve first a linear system whose right-hand side is the *ket* of the matrix element. One then calculates the scalar product between the solution of this linear system and the *bra* [50, 68]. The main limitation of such an approach is that a different linear system has to be solved from scratch for each different value of the frequency. In this thesis we will overcome this difficulty by using the Lanczos algorithm. Such method is an iterative technique commonly used to solve eigenvalue problems or linear systems. The Lanczos procedure builds iteratively a tridiagonal matrix that can give an approximate solution to the full problem; obviously this method is effective because the desired accuracy is reached for a number of iterations which is much smaller than the dimension of the full matrix. Indeed the eigenvalues of relatively small Lanczos tridiagonal matrices can give an approximation of the smallest and largest eigenvalues of the full matrix; by

using the iterative vectors as well, it is possible to obtain the solution of a linear system.

For the sake of clarity, we will start by considering a simplified version of Eq. (2.40), namely a *diagonal* element of the resolvent of a *Hermitian* operator, which can be solved very efficiently by the symmetric Lanczos algorithm [69], avoiding the solution of the linear system altogether [70, 71, 72, 73]. The simplified relation that we want to calculate is written explicitly as

$$g(\omega) = \left\langle v|(\omega - \mathcal{H})^{-1}|v\right\rangle, \tag{2.41}$$

where $\mathcal{H}$ is a Hermitian operator and v is a vector of a n-dimensional space that we suppose to be normalized $\parallel v \parallel = 1$. The Lanczos recursive chain is defined in this way:

$$\beta_1 q_0 = 0, \tag{2.42}$$

$$q_1 = v, \tag{2.43}$$

$$\beta_{j+1} q_{j+1} = \mathcal{H}\ \ q_j - \alpha_j q_j - \beta_j q_{j-1}, \tag{2.44}$$

where $\alpha_j = \langle q_j|\mathcal{H}|q_j\rangle$ and β_{j+1} have to be chosen in order to ensure that $\parallel q_{j+1} \parallel = 1$. This recursion builds a fully orthonormal basis set $\{q_1, q_2, \cdots q_j, \cdots\}$ by simply enforcing the orthonormality condition of vector q_{j+1} to the vectors q_j and q_{j-1}. In the representation of this basis the operator $\mathcal{H}$ becomes a tridiagonal matrix where α_j composes the diagonal and β_j composes the upper and lower diagonals:

$$T^j = \begin{pmatrix} \alpha_1 & \beta_2 & 0 & \cdots & 0 \\ \beta_2 & \alpha_2 & \beta_3 & 0 & \vdots \\ 0 & \beta_3 & \alpha_3 & \ddots & 0 \\ \vdots & 0 & \ddots & \ddots & \beta_j \\ 0 & \cdots & 0 & \beta_j & \alpha_j \end{pmatrix}. \tag{2.45}$$

In this form the operator can be easily inverted to give the continued fraction

$$g(\omega) = \cfrac{1}{\omega - \alpha_1 - \cfrac{\beta_2^2}{\omega - \alpha_2 - \cfrac{\beta_3^2}{\omega - \cdots}}} \tag{2.46}$$

where the Lanczos coefficients α and β have to be calculated only once for all different frequencies. As already anticipated, this technique is very powerful, since the dimension of the iterative space which is necessary to converge to the exact result is much smaller than the dimension of the full linear space. Unfortunately, in finite precision arithmetic, the exact orthonormality of q vectors is not usually preserved and this may lead to instability phenomena.

The generalization of the Lanczos recursion method to non-Hermitian operators is straightforward, based on the Lanczos biorthogonalization algorithm [74, 69]. In this framework it is natural to express an off diagonal element of the resolvent in terms of a continued fraction. Unfortunately, this is less evident in the case in which this element is calculated between two orthogonal vectors. In Ref. [75] such problem were solved using a block version of the Lanczos biorthogonalization. The drawback of this approach is that a different Lanczos chain has to be calculated for the response of each different property to a given perturbation (*i.e.* for each different *bra* in the matrix element corresponding to a same *ket*). Hereafter, we will generalize the recursion method of Haydock, Heine, and Kelly [70, 71, 72, 73], so as to encompass the case of an *off-diagonal* element of the resolvent of a *non-Hermitian* operator, without using any block variant of the algorithm and including the case in which the left and the right vectors are orthogonal. This will allow us to calculate the full dynamical response of *any* dynamical property to a given perturbation, from a single Lanczos chain.

We want to calculate quantities such as:

$$g(\omega) = \left\langle u|(\omega - \mathcal{A})^{-1}v\right\rangle , \tag{2.47}$$

where $\mathcal{A}$ is a non-Hermitian matrix defined in some linear space, whose dimension will be here denoted by n, and u and v are elements of this linear space; for our purposes we suppose v to be normalized $\parallel v \parallel = 1$. For the sake of simplicity, and without loss of generality in view of applications to time-reversal invariant quantum-mechanical problems, we will assume that the linear space is defined over real numbers. To this purpose, let us define a sequence of *left* and *right* vectors, $\{p_1, p_2, \cdots p_k, \cdots\}$ and $\{q_1, q_2, \cdots q_k, \cdots\}$, from the following procedure,

known as the Lanczos *bi-orthogonalization* algorithm [74, 69]:

$$\gamma_1 q_0 = \beta_1 p_0 = 0, \tag{2.48}$$

$$q_1 = p_1 = v, \tag{2.49}$$

$$\beta_{j+1} q_{j+1} = \mathcal{A}\ q_j - \alpha_j q_j - \gamma_j q_{j-1}, \tag{2.50}$$

$$\gamma_{j+1} p_{j+1} = \mathcal{A}^\top p_j - \alpha_j p_j - \beta_j p_{j-1}, \tag{2.51}$$

where:

$$\alpha_j = \langle p_j | \mathcal{A} q_j \rangle, \tag{2.52}$$

and β_{j+1} and γ_{j+1} are scaling factors for the vectors q_{j+1} and p_{j+1}, respectively, so that they will satisfy:

$$\langle q_{j+1} | p_{j+1} \rangle = 1. \tag{2.53}$$

Thus, from an algorithmic point of view, the right-hand sides of Eqs. (2.50-2.51) are evaluated first with α_j as in Eq. (2.52). Then, the two scalars β_{j+1} and γ_{j+1} are determined so that Eq. (2.53) is satisfied. Eq. (2.53) only gives a condition on the *product* of β_{j+1} and γ_{j+1}. If we call $\bar{q}$ and $\bar{p}$ the vectors on the right-hand sides of Eqs. (2.50), (2.51) respectively, this condition is that $\beta_{j+1}\gamma_{j+1} = \langle \bar{q} | \bar{p} \rangle$. In practice one typically sets

$$\beta_{j+1} = \sqrt{|\langle \bar{q} | \bar{p} \rangle|} \tag{2.54}$$

$$\gamma_{j+1} = \text{sign}(\langle \bar{q} | \bar{p} \rangle) \times \beta_{j+1}. \tag{2.55}$$

The resulting algorithm is described in detail, *e.g.*, in Refs. [74, 69]. Let us define Q^j and P^j as the $(n \times j)$ matrices:

$$Q^j = [q_1, q_2, \cdots, q_j], \tag{2.56}$$

$$P^j = [p_1, p_2, \cdots, p_j], \tag{2.57}$$

and let e_k^m indicate the k-th unit vector in a m-dimensional space (when there is no ambiguity on the dimensionality of the space, the superscript m will be dropped). The following Lanczos factorization holds in terms of the quantities calculated from the recursions equations (2.49-2.51):

$$\mathcal{A}\ Q^j = Q^j T^j + \beta_{j+1} q_{j+1} e_j^{j\top}, \tag{2.58}$$

$$\mathcal{A}^\top P^j = P^j T^{j\top} + \gamma_{j+1} p_{j+1} e_j^{j\top}, \tag{2.59}$$

$$P^{j\top} Q^j = I^j, \tag{2.60}$$

where I^j indicates the $(j \times j)$ unit matrix, and T^j is the $(j \times j)$ tridiagonal matrix:

$$T^j = \begin{pmatrix} \alpha_1 & \gamma_2 & 0 & \cdots & 0 \\ \beta_2 & \alpha_2 & \gamma_3 & 0 & \vdots \\ 0 & \beta_3 & \alpha_3 & \ddots & 0 \\ \vdots & 0 & \ddots & \ddots & \gamma_j \\ 0 & \cdots & 0 & \beta_j & \alpha_j \end{pmatrix}. \tag{2.61}$$

In the present case, because of the special block structure of the Liouvillian superoperator and of the right-hand side appearing in Eq. (2.39), at each step of the Lanczos recursion one has that $\mathcal{L}q_j$ is always orthogonal to p_j, so that, according to Eq. (2.52), $\alpha_j = 0$. Let us now rewrite Eq. (2.58) as:

$$(\omega - \mathcal{A})Q^j = Q^j(\omega - T^j) - \beta_{j+1} q_{j+1} e_j^{j\top}. \tag{2.62}$$

By multiplying Eq. (2.62) by $u^\top(\omega - A)^{-1}$ on the left and by $(\omega - T^j)^{-1}e_1^j$ on the right, we obtain:

$$u^\top Q^j(\omega - T^j)^{-1}e_1^j = u^\top(\omega - \mathcal{A})^{-1}Q^j e_1^j - \beta_{j+1} u^\top(\omega - \mathcal{A})^{-1} q_{j+1} e_j^{j\top}(\omega - T^j)^{-1}e_1^j. \tag{2.63}$$

Taking the relation $Q_j e_1^j = q_1 \doteq v$ into account, Eq. (2.63) can be cast as:

$$g(\omega) = \left\langle z|(\omega - T^j)^{-1}e_1^j \right\rangle + \epsilon_j(\omega), \tag{2.64}$$

where:

$$z^j = Q^{j\top}u \tag{2.65}$$

is an array of dimension j, and:

$$\epsilon_j(\omega) = \beta_{j+1} \left\langle u|(\omega - A)^{-1}q_{j+1} \right\rangle \left\langle e_j^j|(\omega - T^j)^{-1}e_1^j \right\rangle. \tag{2.66}$$

is the error made when truncating the Lanczos chain at the j-th step. By neglecting $\epsilon_j(\omega)$ we arrive at the following approximation to $g(\omega)$ defined in Eq. (2.47)

$$\bar{g}_j(\omega) = \left\langle z^j|(\omega - T^j)^{-1}e_1^j \right\rangle \ . \tag{2.67}$$

This approximation is the scalar product of two arrays of dimension j: $\bar{g}_j(\omega) = \langle z^j|w^j\rangle$, where w^j is obtained by solving a tridiagonal linear system:

$$(\omega - T^j)w^j = e_1^j, \tag{2.68}$$

T^j is the tridiagonal matrix of Eq. (2.61), and z^j is given by Eq. (2.65). Two important practical observations should be made at this point. The first is that solving tridiagonal systems is extremely inexpensive (its operation count scales linearly with the system size). The second is that the calculation of the sequence of vectors z_j from Eq. (2.65) does not require the storage of the Q_j matrix. In fact, each component of z^j is the scalar product between one known vector (u) and the Lanczos recursion vector q^j, and it can therefore be calculated on the fly along the Lanczos recursion chain.

From the algorithmic point of view, much attention is usually paid in the literature in finding suitable preconditioning strategies that would allow one to reduce the number of steps that are needed to achieve a given accuracy within a given iterative method [50]. Although preconditioning can certainly help reduce the number of iterations, in general it destroys the nice structure of the Lanczos factorization, Eq. (2.58), which is essential in order to avoid repeating the time-consuming factorization of the Liouvillian for different frequencies. In the next chapter we will show how the extrapolation of the Lanczos coefficient, rather than preconditioning the Liouvillian, leads to a substantial reduction in the number of iterations without affecting (but rather exploiting) the nice structure of the Lanczos factorization, Eqs. (2.59) and (2.58).

We conclude that the non-symmetric Lanczos algorithm allows one to easily calculate a systematic approximation to the off-diagonal matrix elements of the resolvent of a non-Hermitian matrix. It is easily seen that, in the case of a diagonal matrix element, this same algorithm would lead to a continued-fraction representation of the matrix element. Although the representation of Eq. (2.64), which is needed in the case of a non-diagonal element, is less elegant than the continued-fraction one, its actual implementation is in practice no more time-consuming from the numerical point of view.

2.4 A first application to benzene

In order to demonstrate our methodology, we proceed now to the numerical calculation of the spectrum of benzene, a benchmark system for which several TDDFT studies already exist and whose optical spectrum is known to be accurately described by the adiabatic approximation [12, 76, 75, 77]. The resolution of the

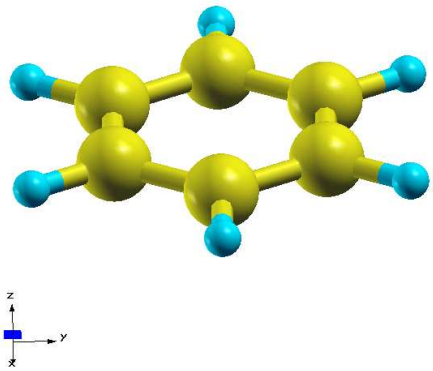

Figure 2.1: The structure of benzene and its orientation in the supercell.

Liouville-Lanczos equations has been implemented in a plane-wave pseudopotential framework as described in appendix A. As a starting ingredient of a calculation, only the occupied states are required. The overall numerical scalability of the algorithm is not different from that of an iterative ground-state calculation, since the necessary operations (Hamiltonian-vector multiplication and Hartree potential evaluation) are exactly the same. For the simulation of benzene we used a tetragonal supercell whose dimensions are $30 \times 30 \times 20$ au^3. The orientation of the molecule in the supercell is shown in Fig. 2.1.

Calculations have been performed using the LDA functional as parametrized by Perdew and Zunger [59]. Norm-conserving pseudopotentials have been used with a kinetic-energy cutoff of 60 Ry, which corresponds to 70600 PW's. The dimension of the Liouvillian superoperator exceeds 2 million. A small imaginary part has been added to the frequency argument, $\omega \rightarrow \omega + i\eta$, in order to solve the linear system Eq. (2.68). This shift into the complex frequency plane has the effect of introducing a Lorentzian broadening in the discrete spectral lines. In the continuous part of the spectrum the truncation of the Lanczos chain introduces a spurious discretization of the spectrum, which appears then as the superposition of discrete peaks. The choice of a relatively large (depending on the dimension of the basis set) value for the broadening η has the effect of correcting this feature, thus re-establishing the continuous character of the spectrum. If the chosen value

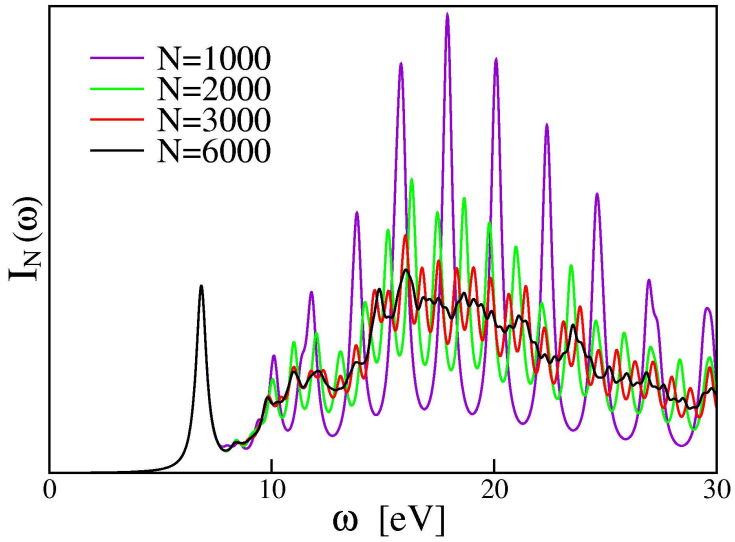

Figure 2.2: Absorption spectrum of benzene between 0 and 30 eV shown for different numbers of Lanczos recursion steps N.

of η is too large, some of the features of the discrete spectrum can be hidden by the superposition of Lorentzian broadenings. In the next chapter, this problem is solved using a technique that allows an inexpensive extrapolation of Lanczos coefficients up to a very large order. In this way a small broadening can be used avoiding the effect of the finite length of the Lanczos chain in the continuous spectrum. Throughout this first benchmark we have set $\eta = 0.02$ Ry in order to obtain a better comparison with experimental data.

The convergence properties of the algorithm are illustrated in Fig. 2.2, which shows that about 6000 iterations are necessary to obtain a fully converged spectrum between 0 and 30 eV. First of all we note that the low-energy part converges faster than the high-energy part. Secondly, we have found that there is a dependence between the kinetic energy cutoff and the convergence of the spectrum. Namely, the smaller the cutoff the faster the convergence. Therefore the possibility of using a smaller basis set is crucial in order to broaden the range of applicability of the method. For this reason our approach has also been implemented in an ultrasoft pseudopotential scheme (details are given in Appendix B). The convergence of the benzene spectrum in the ultrasoft case is shown in Fig. 2.3. In this case we have used a GGA functional, to be specific the Perdew-Burke-

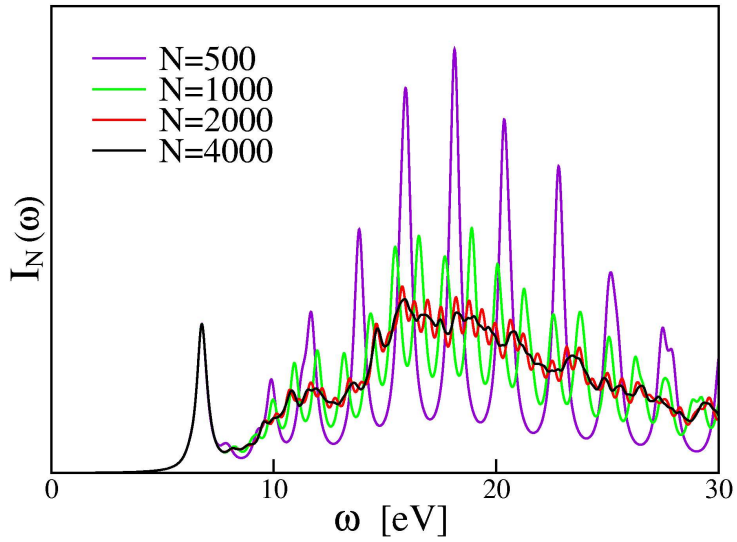

Figure 2.3: Absorption spectrum of benzene between 0 and 30 eV calculated using ultrasoft pseudopotentials. The figure shows the curve for different numbers of Lanczos recursion steps N.

Ernzerhof (PBE) [62]. A cut-off of 30 Ry (180 Ry for the charge density) has been used; this corresponds to about 25000 PW's and to a dimension of the Liouvillian super-operator that almost reaches 750000. In this case the number of iterations necessary to converge is substantially smaller compared to the norm-conserving case and it lies between 2000 and 3000. For this reason, hereafter, we will only use the ultrasoft approach for our calculations. In the present case the spectrum does not change significantly if using adiabatic LDA or adiabatic GGA (this is particularly evident in Fig. 2.4).

A comparison of the performance of our method with Casida's approach is not straightforward and meaningful. Indeed, the target of the two methods is different. With Casida's equations it is possible to calculate each individual excitation and to assign it qualitatively to a specific transition. In general this operation is feasible only in a restricted energy range, which is not typically larger than 10 eV and which depends also on the density of the excitation energies. Differently, with our method we can compute the absorption spectrum in a really wide energy range but we miss a systematic way to assign the transitions. Instead, the comparison with the real-time method is more direct. In our approach, as well as in the

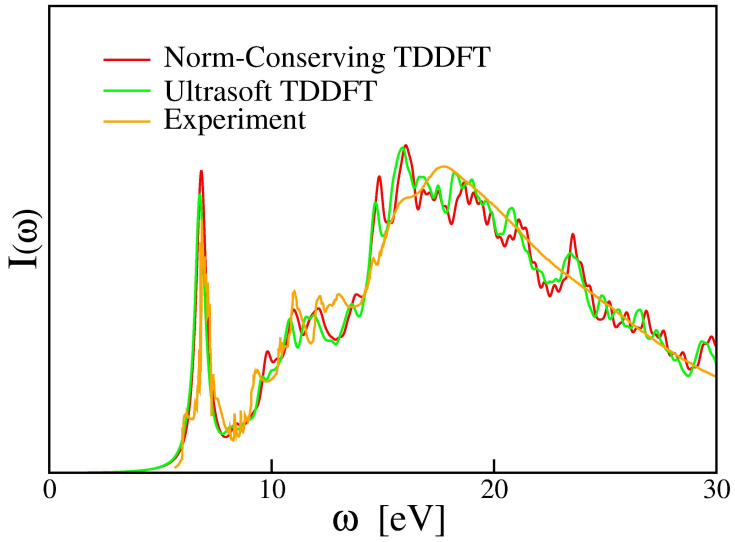

Figure 2.4: Comparison of the TDDFT absorption spectrum of benzene calculated with norm-conserving and ultrasoft pseudopotentials with experimental results. Theoretical results have been scaled so as to obtain the same integrated intensity as experimental data.

real-time approach, the calculation does not require an explicit diagonalization of the full ground-state Hamiltonian. Another similarity consists in the fact that both methods have a numerical scalability comparable to that of ground-state calculations. Indeed at each iteration the required operations consist in the evaluation of at least one Hartree potential and in a certain number of Hamiltonian-wave function ($H\Psi$) products. From this point of view our method requires only two $H\Psi$ products while in the real-time approach the number is sensibly larger (depending in any case on the integration scheme adopted). In general also the number of iterations in real-time applications is larger. To demonstrate this point we can compare the ultrasoft test on benzene with a similar one performed in a real-time PW-USPP implementation [77]. In that calculation a smaller kinetic-energy cutoff was used but a larger number of integration steps was necessary. Each one of the three initial states (corresponding to different polarizations) was propagated for 5000 iterations with a Cranck-Nicolson integration scheme. If we consider that each one of these steps requires several more applications of the Hamiltonian to a vector than the two used in our method, we conclude that our approach is

much more efficient in linear response calculations.

The agreement of our results with experimental data is also good, as shown in Fig. 2.4. This was already known from previous calculations on benzene [12, 76, 75, 77]. Indeed the low lying part of the spectrum is characterized by $\pi \longrightarrow \pi^\star$ transitions which are slightly affected by the incorrect asymptotic behavior of AXCA.

Chapter 3

Testing and improving the numerical efficiency

In this chapter we will analyze the numerical properties of the Liouville-Lanczos method in detail. This analysis will suggest a suitable extrapolation scheme that allows for a dramatic decrease in the number of iterations necessary to achieve convergence. This approach is applied to calculate in a wide energy range the optical properties of large molecular systems, such as fullerene C_{60} *and chlorophyll.*

3.1 Numerical properties of the Liouville-Lanczos method and extrapolation of the Lanczos coefficients

In this section we come back to the ultrasoft benchmark test of benzene considered in Sec. 2.4. Our purpose here is to focus more deeply on the numerical properties of the Liouville-Lanczos equations and to investigate possible improvements in our methodology. Let us start our analysis by considering the Lanczos coefficients z_j, β_j and γ_j, as defined by Eqs. (2.65), (2.54), and (2.55) respectively. In Fig. 3.1 we report their behavior as functions of the Lanczos iteration count, calculated when the direction of both the perturbing electric field and the observed molecular dipole are parallel to each other and aligned along the x direction (this would correspond to the xx component of the polarizability tensor). We can see that the

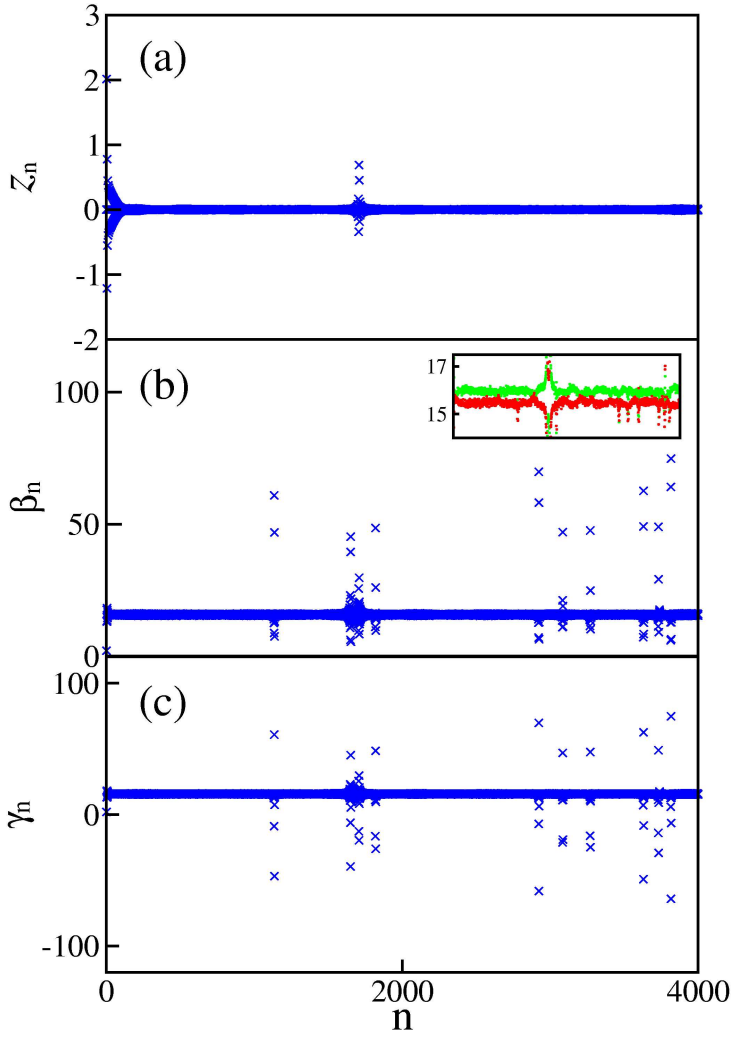

Figure 3.1: (a) Numerical behavior of the components of the z^j vector given by Eq. (2.65). Apart from some out of scale oscillations, they tend rapidly to a value near zero. (b) Numerical behavior of β_j coefficients given by Eq. (2.54). They tend rapidly to a constant value even if some out of scale oscillation is present. In the inset the same data are shown on a different scale and with different colors for odd (green) and even (red) coefficients. (c) The γ_j coefficients given by Eq. (2.55), which can assume the value $\pm\beta_j$. The plot shows that γ_j and β_j have a different sign only in correspondence with few recursion steps.

z's rapidly tend towards zero, whereas the β's tend to a constant. Closer inspection of the behavior of the latter actually shows that the values of the β's are scattered around two close, but distinct, values for even and odd iteration counts. This specific feature is shown in the inset of Fig. 3.1(b). The γ's, which can assume the value $\pm\beta$, only rarely become negative.

From Fig. 3.1 it is also evident that, in correspondence with some iterative steps, wild oscillations occur, namely the coefficients move away from their (almost) constant value. For the coefficients γ_j and β_j this case can be partly explained by their definitions, namely Eqs. (2.54) and (2.55). It can be noticed that there is the possibility for Eq. (2.54) to become zero and this would lead to a division by zero in the algorithm. The occurrence of a zero scalar product $\langle\bar{q}|\bar{p}\rangle$ is known as a *breakdown*. Several situations can take place in this case. For example a *lucky* breakdown occurs when one of the vectors $\bar{q}$ or $\bar{p}$ is zero. If $\bar{q} = 0$ the approximate solution of the linear system associated to the non-symmetric matrix $\mathcal{A}$ is exact; this result holds for $\mathcal{A}^\top$ when $\bar{p} = 0$. Another well-known situation, which is more suitable to explain what happens in our case, arises when neither $\bar{q}$ nor $\bar{p}$ are zero but their inner product is exactly zero. This situation has been studied extensively in the literature [78, 79, 80]. One of the main results is that when this kind of breakdown takes place, for example, at step j, then it is often possible to continue the algorithm by essentially bypassing step j and by computing q_{j+2}, p_{j+2} or some q_{j+l}, p_{j+l} where $l > 1$ directly. Intermediate vectors are needed to replace the missing $q_{j+1}, ...q_{j+l-1}$ and $p_{j+1}, ...p_{j+l-1}$, but these vectors are no longer bi-orthogonal and as a result the tridiagonal matrix will have "bumps" in its upper part. The class of algorithms devised for this situation are called "look-ahead Lanczos" algorithms (LALA's) [78]. Sometimes this LALA procedures cannot be applied and this situation is defined as *incurable breakdown.* Note that this type of breakdown does not occur in the Hermitian Lanczos process. It is a manifestation of the existence of vectors in the right subspace (vector space spanned of Q^j) that are orthogonal to all vectors of the left subspace (vector space spanned of P^j), which is impossible when these spaces are the same ($Q^j = P^j$ in the Hermitian case). Clearly, in finite precision calculations, exact breakdowns (inner product $\langle\bar{q}|\bar{p}\rangle$ exactly equal to zero) are extremely rare. Nevertheless, it could be necessary to apply LALA procedures also in the case of a near-breakdown, namely when $\langle\bar{q}|\bar{p}\rangle$ becomes small.

In our calculations we never found that $\langle\bar{q}|\bar{p}\rangle$ reaches a value that is really close to zero, but sometimes it decreases under its (nearly) constant value and, as a consequence, the norm of Lanczos vectors becomes very large as in a real break-down situation. The large norm of the new Lanczos vectors is responsible for the increase of $\langle\bar{q}|\bar{p}\rangle$ in the subsequent iterations (this explains the values of β and γ larger than the constant). We also noted that the occurrence and position of these instabilities could depend on the details of the calculation (e.g. numerical routines) but the final spectrum is robust and independent of these details. In our experience these near-breakdown phenomena do not seem to affect the stability properties of our algorithm. Instead, convergence properties are likely to be slowed down by the loss of information due to the increase of the norm of Lanczos vectors. Nevertheless, there are good reasons not to use LALA techniques to deal with instabilities. The T^j matrices generated by LALA are not tridiagonal. Furthermore, a proper implementation of LALA's would require saving a number of vectors (the number l above) which is not known in advance; this could pose a serious problem because of the large dimension of the linear spaces we use. Finally, we can note that the components of z^j can also show jumps in their magnitude, since the norm of the Lanczos iterative vectors occasionally display large variations.

In general the algorithm we use does not seem significantly affected by the loss of orthogonality (more properly biorthogonality) of the iterative vectors. This is a well-known problem, which strongly limits the applicability of Lanczos techniques in the solution of eigenvalue problems. In fact, by using our method, we are not really solving an eigenvalue problem; rather, we use the Lanczos recursion to implicitly solve a linear system. The fact that the solution of linear systems is not sensitively affected by the loss of orthogonality has not been understood completely but it is already well-known for the Bi-conjugate gradient algorithm (BiCG), which is mathematically equivalent [69] to the Lanczos procedure we use. In BiCG the underlying vectors loose their theoretical orthogonality and the scalars used for the recurrences may undergo very large oscillations; nevertheless the iterates generated to solve the linear system usually converge quite well.

The fast decrease in the components of z^j implies that the quality of the calculated spectrum only depends on the first few hundreds of them. Namely, if we set the components of the z^j vector equal to zero in Eq. (2.64) after, say, 300-400

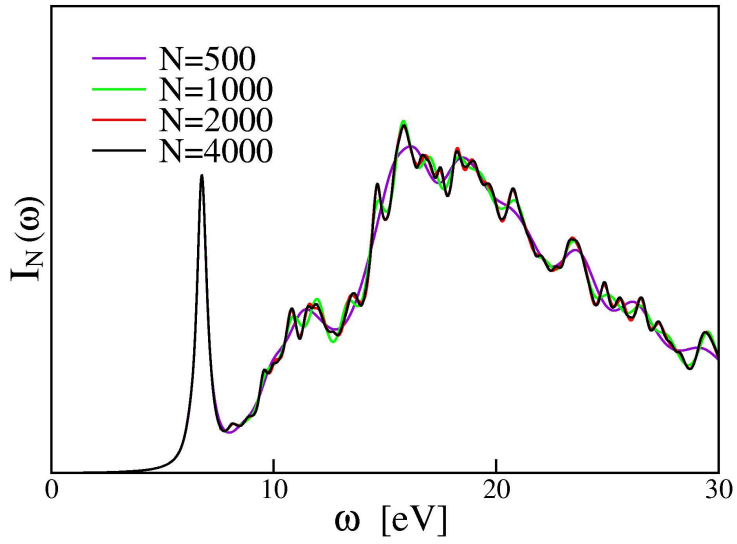

Figure 3.2: Convergence of the absorption spectrum of benzene using the extrapolation procedure described in the text. After N iterations the components of z^j are set to zero and the β's are extrapolated.

iterations, but we keep the dimension of the tridiagonal matrix, T^j, on the order of 2-3000, the resulting spectrum still appears to be perfectly converged. Unfortunately, a relatively large number of iterations seems to be necessary to calculate a tridiagonal matrix of adequate dimensions. The regular behavior of the β's for large iteration counts suggests an inexpensive strategy to extrapolate the Lanczos recursion. Let us fix the dimension of the tridiagonal matrix in Eq. (2.64) to some very high value (say, $j = 10000$), and define an effective z^j vector, z^j_N, and T^j matrix, T^j_N, by setting the k-th component of z^j_N equal to zero for $k > N$, and the k-th component of β equal to the appropriate estimate of the asymptotic value for odd or even iteration counts, obtained from iterations up to N. In general there are only a few iterative steps where γ_j has a sign different from that of β_j; therefore we use the same extrapolation for both coefficients. In Fig. 3.2 we display the spectra, $I_N(\omega)$, obtained from the extrapolation procedure which has just been outlined. One sees that the extrapolated spectrum is already at perfect convergence for a modest value of N in between $N = 500$ and $N = 1000$; this is a substantial improvement with respect to the results shown in Fig. 2.3. Note that this extrapolation procedure, apart from the enhancement of convergence, also of-

fers an efficient solution to the problem of recovering a continuous spectrum from a limited number of recursion steps. As the dimension of the tridiagonal matrix appearing in Eq. (2.64) can be increased arbitrarily at a very small cost, the distance between neighboring pseudo-discrete eigenvalues in the continuous part of the spectrum can be reduced correspondingly; as a consequence, the imaginary part of the frequency can be basically chosen as small as wanted.

A qualitative insight into the asymptotic behavior of the Lanczos recursion coefficients can be obtained from the analogy with the continued-fraction expansion of the local density of states (LDOS) for tight-binding Hamiltonians, a problem that has been the breeding ground of the application of Lanczos recursion methods to electronic-structure theory. It has been known since the late seventies that the coefficients of the continued-fraction expansion of a *connected* LDOS asymptotically tend to a constant (which equals one fourth of the band width) whereas they oscillate between two values in the presence of a gap: in the latter case the average of the two limits equals one fourth of the total band width, whereas their difference equals one half of the energy gap [81]. These results can be easily verified in the case of a continued fraction with constant hopping parameter, β:

$$g(\omega) = \cfrac{1}{\omega - \cfrac{\beta^2}{\omega - \cfrac{\beta^2}{\omega - \cdots}}} \tag{3.1}$$

$$= \frac{\omega \pm \sqrt{\omega^2 - 4\beta^2}}{2\beta^2}, \tag{3.2}$$

where the sign has to be chosen so as to make the Green's function have the proper imaginary part. In this case, one sees that the imaginary part of the Green's function (which equals the LDOS) is non-vanishing over a band that extends between -2β and 2β. In the case in which consecutive hopping parameters of the recursion chain oscillate between two values, β_1 and β_2, the resulting Green's function reads:

$$g(\omega) = \cfrac{1}{\omega - \cfrac{\beta_1^2}{\omega - \cfrac{\beta_2^2}{\omega - \cdots}}} \tag{3.3}$$

$$= \frac{\omega^2 + \beta_1^2 - \beta_2^2 \pm \sqrt{(\omega^2 + \beta_1^2 - \beta_2^2)^2 - 4\omega^2\beta_1^2}}{2\omega\beta_1^2}; \tag{3.4}$$

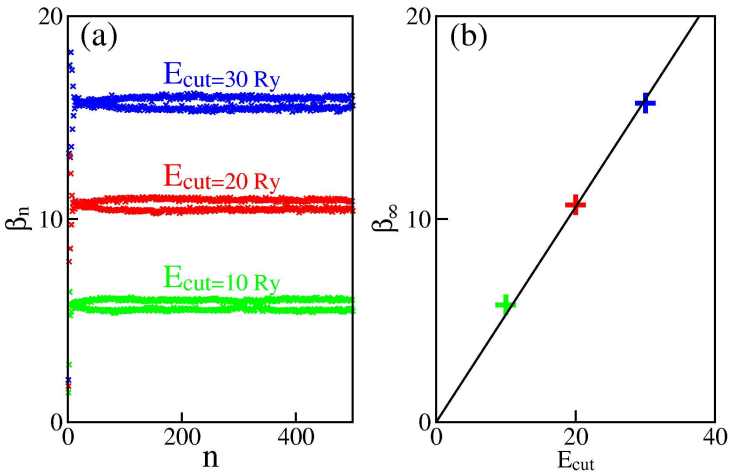

Figure 3.3: (a) Behavior of β's coefficients for different values of the kinetic energy cut-off. (b) The asymptotic values β_∞ plotted as a function of the kinetic energy cut-off; the figure shows that they can be connected by a straight line with a slope of about 0.5.

in this case we obtain two bands between $|\beta_1 - \beta_2|$ and $\beta_1 + \beta_2$ and between $-(\beta_1 + \beta_2)$ and $-|\beta_1 - \beta_2|$.

In our case, the band width of the Liouvillian super-operator extends from minus to plus the maximum excitation energy, which is of the order of the PW kinetic-energy cutoff E_{cut}. The gap, instead, is of the order of twice the optical gap Δ. Because of Eq. (3.4), we expect that the asymptotic values of the β (and similarly γ) coefficients of the Liouville Lanczos chain qualitatively satisfy the relations $\beta_\infty^{odd} + \beta_\infty^{even} = 2\beta_\infty \approx E_{cut}$ and $|\beta_\infty^{odd} - \beta_\infty^{even}| \approx \Delta$. In Fig. 3.3(a) we report the behavior of the values of the β coefficients of the Lanczos chain calculated for benzene, *vs.* the iteration count, for different kinetic energy cut-off. In Fig. 3.3(b) the average asymptotic value β_∞ is plotted as a function of the kinetic energy cut-off, thus demonstrating a linear dependence $\beta_\infty \approx \frac{1}{2}E_{cut}$, in remarkable agreement with the above-mentioned prediction. The difference between the asymptotic values of odd and even coefficients $|\beta_\infty^{odd} - \beta_\infty^{even}| \approx 0.46\text{Ry}$ is also in qualitative agreement with the optical gap which we have found to be 0.38Ry.

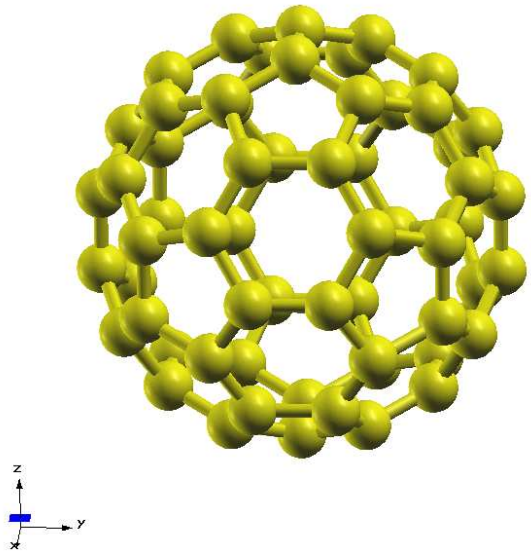

Figure 3.4: The structure of fullerene C_{60} and its orientation in the supercell.

3.2 Application to fullerene

In this section we apply our method to a much more challenging problem such as the spectrum of fullerene C_{60}. Here, and in the next section, we show that our approach, despite the large dimension of the basis set, is able to calculate spectra on a wide range of energies and the results compare well with other theoretical and experimental data.

Fullerene C_{60} has already been the subject of experimental [17, 82] and theoretical [15, 16, 17, 18, 12, 19] studies; therefore, it is a good benchmark for our method. The molecule has been placed in a cubic supercell with a side length of 35 au and the calculation has been performed using the PBE functional [62] and ultrasoft pseudopotentials with a kinetic energy cut-off of 30 Ry and with a charge density cut-off of 180 Ry. The dimension of the basis set reaches almost 60000 PW's and the dimension of the full Liouvillian exceeds 14 million. As in the previous calculations, a Lorentzian broadening of 0.02 Ry is added to solve the linear system. In Fig. 3.5(a) the absorption spectrum between 0 and 40 eV is shown. The Lanczos recursion is explicitly computed up to some order N and extrapolated, afterwards, up to 20000. This specific value has been chosen rather

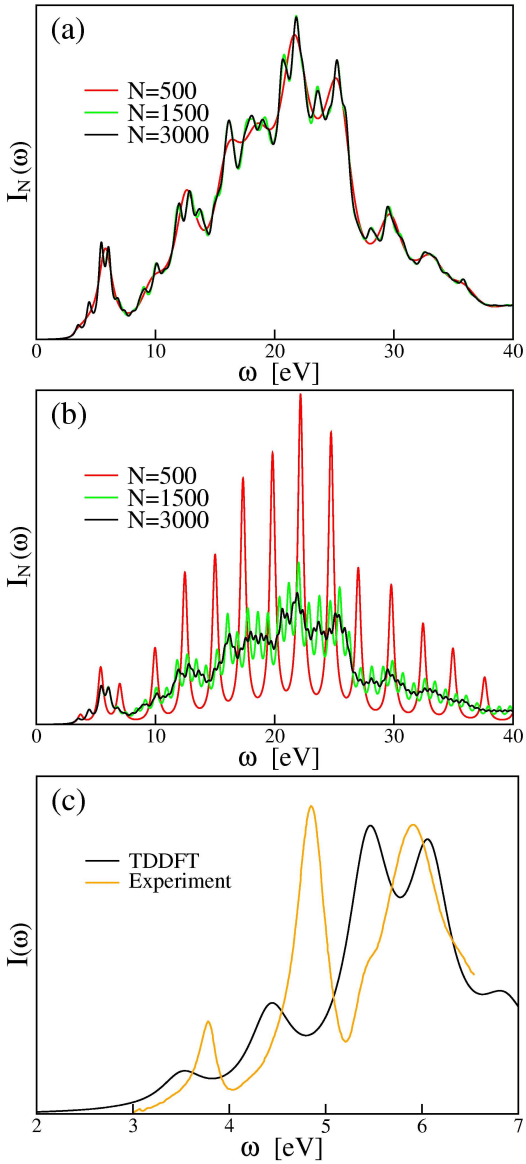

Figure 3.5: (a) Convergence properties of the absorption spectrum of fullerene calculated between 0 and 40 eV using the Lanczos extrapolation technique. (b) The same spectrum as above obtained without the extrapolation scheme. Small ripples are still present even after 3000 iterations. (c) The fully converged absorption spectrum of fullerene compared with experimental results [17] in the energy range between 2 and 7 eV. TDDFT results are scaled so as to obtain the same integrated intensity as the experiment.

arbitrarily to ensure full convergence. The results are already qualitatively good after only N=500 and practically perfect after N=1500. If we do not use this Lanczos coefficients extrapolation, as in Fig. 3.5(b), after 500 iterations we have huge oscillations in the spectrum and small ripples are still present after 3000 iterations. For this reason the use of the bi-constant terminator is of formidable importance to reach convergence.

The overall shape of the spectrum is in substantial agreement with the spectra calculated in a wide energy range in Ref. [16, 12, 18]. In that calculations the spectrum is obtained using real-time propagations of the TDDFT equations; within this approach the possibility of extending the calculation to a wide energy range is due to the use of a smaller integration time step (with an evident increase in computational cost); in our case, by using the termination of the Lanczos chain, this problem is not relevant at all. A direct comparison with the performance of Ref. [16, 12, 18] is not possible since in Yabana and Bertsch a real grid implementation is used and in Tsolakidis *et al.* equations are expanded on a basis of numerical orbitals. However, the fact that in the first case 30-40000 iterations are used and in the second more than 6000 seems to suggest, again, that the number of the expensive Hamiltonian-wave function multiplications is largely smaller in our approach.

The main features of the C_{60} spectrum are the low-energy part of the spectrum characterized by the transitions of π electrons and the broad region between 14 eV and 27 eV where transitions come from σ and π electrons. The low frequency part of the spectrum is explicitly compared with the experimental results of Bauernschmitt *et al.* [17] in Fig. 3.5(c). The intensities are not perfectly reproduced, but the main transitions compare well, apart from a slight redshift, as already found in Ref. [17].

3.3 Application to chlorophyll a

An even more challenging test is chlorophyll, a molecule which is of fundamental importance for life on Earth since it is responsible for the photosynthetic process. There are several different forms of this molecule but we will focus on chlorophyll a. Historically the interpretation of the visible spectrum of chlorophyll relies on the 4-orbital Gouterman model of porphyrins [83] in which only the two highest

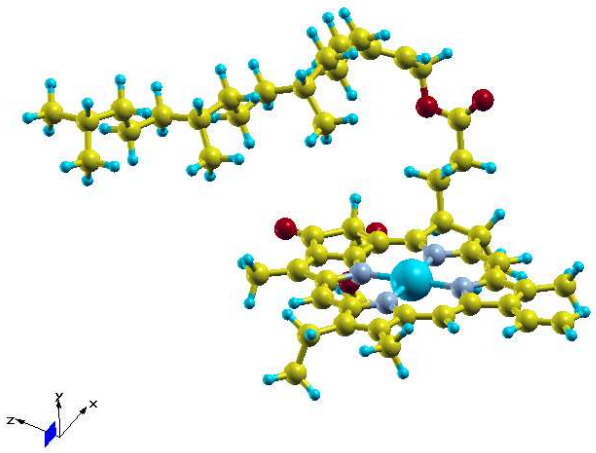

Figure 3.6: The structure of chlorophyll a and its orientation in the supercell.

occupied molecular orbitals and the two lowest unoccupied molecular orbitals are considered. In the last few years there have been several calculations of its low energy spectrum relying on different $ab\ initio$ techniques [7, 8, 84, 9, 10, 85]. Despite the fact that adiabatic TDDFT seems to produce spurious charge transfer states in the visible region [9], we will see that in our application the overall shape of the low energy spectrum seems to be substantially correct. For our calculations we have placed the molecule in a super-cell of the following dimensions: $35 \times 45 \times 55$ au^3; the PW91 functional [61] has been used together with ultrasoft pseudopotentials with a kinetic energy cut-off of 30 Ry and a charge density cut-off of 180 Ry. The KS orbitals are expanded over more than 120000 PW's and the dimension of the Liouvillian super-operator exceeds 40 million. In this case a Lorentzian broadening of 0.002 Ry has been added to the transition energies to obtain a better comparison between our results and experiments. In Fig. 3.7(a) the convergence of the spectrum calculated in a wide range of energy between 0 and 40 eV is shown; the usual bi-constant termination is added. In this case we notice that convergence requires a larger number of iterations in order to reproduce the detailed features of the spectrum. This is connected to the use of a smaller

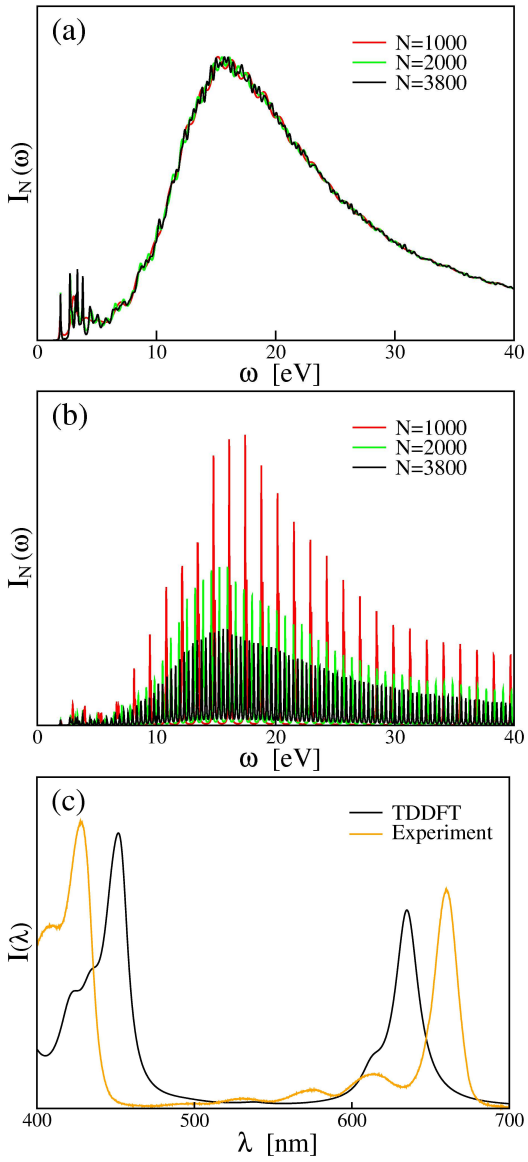

Figure 3.7: (a) Convergence of the chlorophyll absorption spectrum between 0 and 40 eV using the Lanczos chain extrapolation. (b) Convergence without extrapolation. (c) Chlorophyll absorption spectrum in the visible region between 400 and 700 nm compared with the experimental data in diethyl ether of Ref. [86]. As usual the computational results have been scaled in order to obtain the same integrated intensity as experimental results.

Lorentzian broadening. In Fig. 3.7(b) the same results are shown without adding the extrapolation of the Lanczos coefficients. In this case the overall convergence is insufficient, even after N=3800. The lack of states in the continuous part of the spectrum is particularly evident since it causes a pseudo-discretization of the excitations evident in the plot. This lack is easily compensated by the use of the Lanczos chain termination. In Fig. 3.7(c) we compare the visible part of the spectrum calculated in this work with the experimental results obtained in diethyl ether solution in Ref. [86]. A good agreement with the experiment is clearly observed but the Soret (B) band located at 430 nm in the experiment is slightly red-shifted in the calculation and the red band (Q) has an opposite behavior. How much of this discrepancy has to be attributed to the limitations of the AXCA alone, or to a combination of them with the neglect of solvation effects remains to be ascertained. The experimental weak transitions between the two main peaks are not well reproduced; in that energy range other TDDFT calculations have found very small oscillator strengths, which, in our case, are most probably hidden by the Lorentzian broadening.

Chapter 4

TDDFT study of squaraine dye-sensitized solar cells

In this chapter we will apply the Liouville-Lanczos method to the study of dye-sensitized solar cells, which are very promising devices to exploit the energy of solar light. As an example, we will consider $\mathrm{TiO_2}-$*supported squaraine dyes, which are interesting candidates to broaden sensitization in the red spectral region, and we will discuss the underlying mechanisms that rule the functioning of these devices.*

4.1 Dye-sensitized solar cells

In a world where the energetic problem is increasingly important, research on alternative energy sources has become of fundamental value. One of the most interesting renewable sources of energy is represented by solar light. A breakthrough in its exploitation was the introduction of Dye Sensitized Solar Cells (DSSC's) [55], which have attracted considerable interest since they combine a relatively high efficiency with very low production costs. DSSC's consist of dye molecules adsorbed on the surface of a film or of nanoparticles composed of a large gap semiconductor, such as $\mathrm{TiO_2}$ (the most widespread support and the one we will consider hereafter). The key process in the functioning of DSSC's is the injection of light-excited electrons from the dye into the conduction band of the semiconductor. This process depends on the structure of the dye/semiconductor interface,

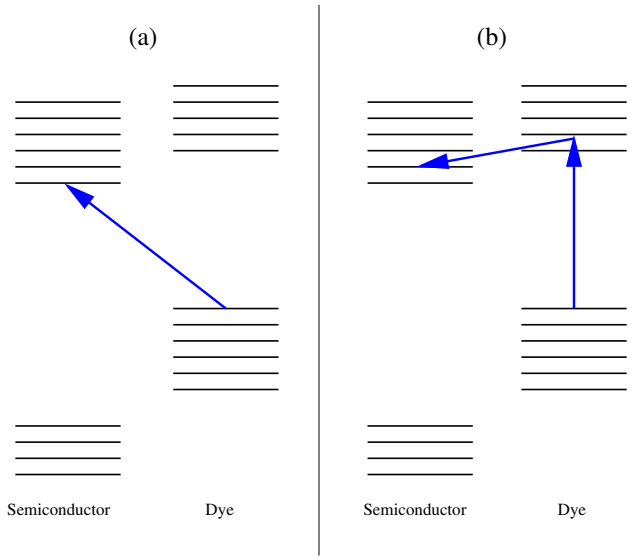

Figure 4.1: Sketch of the alignment of the energy levels of the dye and of the semiconducting substrate in a DSSC. (a) Direct transition mechanism in DSSC's; (b) indirect mechanism (see text).

and on the precise nature of the involved electronic excited states.

In Fig. 4.1 the alignment of the dye and of substrate energy levels which occurs in a typical DSSC is shown qualitatively. In general, the HOMO (highest occupied molecular orbital) of the DSSC system corresponds to a molecular state and the LUMO (lowest unoccupied molecular orbital) to an electronic state of the substrate; the net effect is a lowering of the energy gap of the overall system with respect to that of the semiconductor substrate. Given this alignment of the energy levels, the injection of one electron into the substrate can have different underlying mechanisms. Indeed, we can have a direct transition from the occupied levels of the dye to the conduction band of the TiO_2 substrate (direct mechanism), or the absorption of a photon from within the dye, followed by the transfer of the photo-excited electron into the semiconductor conduction band (indirect mechanism). This mechanism is in general more efficient since it can involve more than one final state in the TiO_2 conduction band. In this case, in order to achieve high electron transfer quantum yields, the dye needs to be strongly coupled to the semiconductor and it has to produce long-lived excited states with energies that almost match those of the TiO_2 conduction band. After injection, it is necessary to close

the circuit in order to generate a current. This is achieved through an electrolyte (which can be also substituted by a p-type semiconductor) and a counter-electrode (the electrode, instead, is the TiO_2 substrate). When an electron is injected from the dye into the semiconductor, a new electron is provided by the electrolyte, thus closing the circuit. This process takes place without any chemical transformation of the dye.

A breakthrough in the DSSC's technology has been determined by the extraordinary performance of *cis*-di(thiocyanato)bis(2,2'-bipyridyl-4,4'-dicarboxylate)ruthenium(II) sensitizer (N3) attached to nanocrystalline TiO_2 films [55, 87, 88]. Indeed this system has a 10% solar-to-electric power conversion under AM 1.5 (AM indicates the Air Mass.). Ruthenium complexes are still the most widespread dyes in this kind of application, but research to optimize the dye is extremely active. Ruthenium complexes absorb visible light mainly around 2.3 eV. For this reason, in order to further improve the performance of DSSC's, it is necessary to fit better the absorption band of the dye with the solar spectrum. The introduction of dyes that enhance absorption in the red/near infrared region is, therefore, of fundamental importance. From this point of view squaraines are good candidates for their strong absorption in that energy range. Different experimental applications already exist [89, 90, 91, 92, 93, 94]. In [94] a new asymmetrical squaraine was introduced, with a carboxilic acid group to anchor the molecule to a 4 μm TiO_2 film. Under standard solar conditions AM 1.5, the solar cell built this way has reached an overall efficiency of 4.5%. The importance of studying these molecules is also connected with the possibility of cosensitization of different dyes with a different spectral response. Indeed in [95] a series of squaraines have been applied together with ruthenium complexes to obtain a substantial improvement of the photon-current conversion efficiency.

The main theoretical challenge concerning DSSC's is to understand the mechanisms that rule their functioning at the atomic scale, with the final purpose of engineering new dyes with custom-tailored optimal properties. As we have already remarked, a fundamental characteristic of DSSC's is the proper alignment of the energy levels of the dye with the substrate levels. TDDFT can be a suitable approach to address this problem and applications to DSSC's already exist [30, 31]. In the next section we will apply the Liouville-Lanczos method to a model of the squaraine-based DSSC considered in [94]. We will also address the

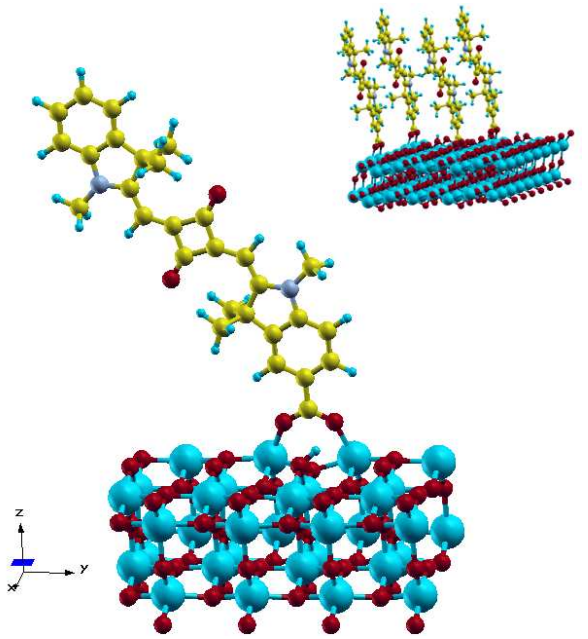

Figure 4.2: Translational unit of the squaraine DSSC model, consisting of the molecule adsorbed on a two-layer slab. The system is oriented with the z axis perpendicular to the slab surface.

problem of the assignment of a transition mechanism.

4.2 A numerical study of a squaraine DSSC

In this section we will consider the computational study of squaraine dye-sensitized solar cells. Squaraines are a class of organic dyes with intense absorption of radiation in the red/near infrared energy range. Such molecules are characterized by a squaric acid core; this acid has the chemical formula $\mathrm{C_4H_2O_4}$, with the four carbon atoms forming a square. The specific dye we consider is 5-Carboxy-2-[[3-[(1,3-dihydro-3,3-dimethyl-1-ethyl-2H-indol-2-ylidene)methyl]-2-hydroxy-4-oxo-2-cyclobuten-1-ylidene]methyl]-3,3-trimethyl-1-octyl-3H-indolium, which has been introduced in Ref. [94]. The carboxylic group (-COOH) is used to anchor the molecule to the $\mathrm{TiO_2}$ substrate. In general $\mathrm{TiO_2}$ can crystallize in three different forms, namely anatase, rutile, and brookite; the first of these is the most widespread in DSSC's applications, since it has shown a better performance

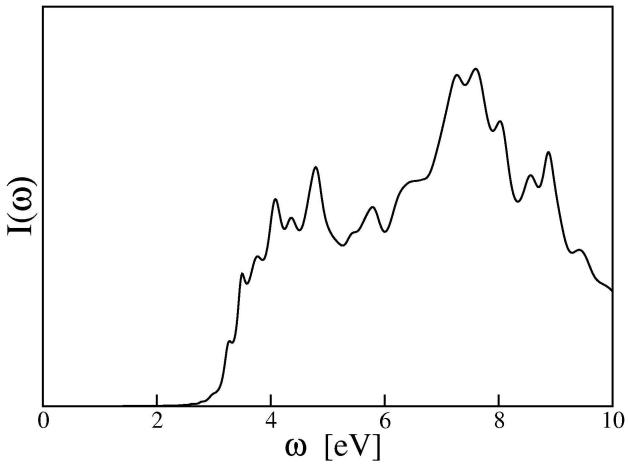

Figure 4.3: Absorption spectrum of the TiO_2 slab, as calculated from TDDFT between 0 and 10 eV.

[96, 97].

Our model consists of the molecule adsorbed on a two-layers periodically repeated TiO_2 slab; the translational unit is shown in Fig. 4.2. The structure of the squaraine has been simplified by replacing the octyl substituents with methyls. The exposed surface of the slab is the (101) of the anatase structure, using a (1×4) primitive cell. The dimension of the cell containing the system is $19.35 \times 28.61 \times 54.28$ au^3. We also performed the simulation of the isolated slab and of the isolated molecule in cells of dimension $19.35 \times 28.61 \times 45.66$ au^3 and $52.91 \times 26.46 \times 23.62$ au^3 respectively. The calculations have been performed considering only the Γ point in the first Brillouin zone. We used the Perdew-Burke-Ernzerhof (PBE) [62] xc functional, ultra-soft pseudopotentials and a PW basis set, up to a kinetic energy cut-off of 25 Ry and 200 Ry for the charge density. An imaginary part of 0.002 Ry has been added to the frequency. To calculate the spectra we used the extrapolation of Lanczos coefficients illustrated in the previous chapter.

First of all we have to consider the reliability of the optical properties of the model used for the TiO_2 substrate. Indeed the slab must not absorb in the visible region in order to reproduce the characteristics of the real system. The KS HOMO-LUMO gap of the slab is equal to 2.5 eV and remains substantially unaffected in the TDDFT calculation; even smaller is the gap of the anatase bulk,

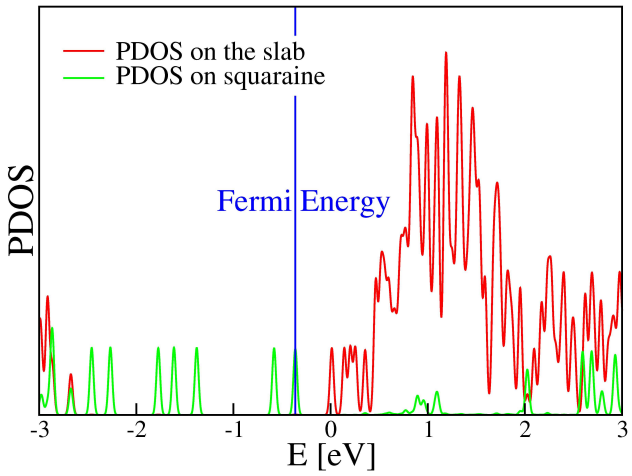

Figure 4.4: Electronic density of states of our DSSC model, as projected on the TiO_2 slab and on the squaraine molecule.

equal to 2.16 eV. Both this values are sensibly lower than the experimental value of 3.2 eV for the bulk. This is a manifestation of the well-known gap problem of GGA functionals [98]. Nevertheless, the calculated absorption spectrum in Fig. 4.3 shows a very low intensity in the visible region, and we thus consider our slab an acceptable model for the substrate.

In order to ascertain the proper alignment of the molecular electronic states with those of the substrate, we calculate the density of Kohn-Sham states for the full DSSC system, projected onto the dye and the substrate components (PDOS), as shown in Fig. 4.4. We obtain the expected behavior for a DSSC, since the HOMO is a purely molecular state while the LUMO is an electronic state of the slab. It is also important to note that the unoccupied molecular states lie in a region where the states of the slab are dense, thus tending to hybridize with the latter. This feature is also evident in the visualization of the isosurfaces of the KS orbitals, which has not revealed the presence of purely molecular orbital in the conduction band.

We are now ready to move on to the optical properties of the squaraine DSSC. Before considering the TDDFT results, let us describe some experimental findings. Fig. 4.5(a) shows that, in the visible region, squaraine presents a strong absorption peak around 1.94 eV, which corresponds to a $\pi \rightarrow \pi^\star$ transition. When the molecule is adsorbed on a 4 μm TiO_2 film the main features do not signifi-

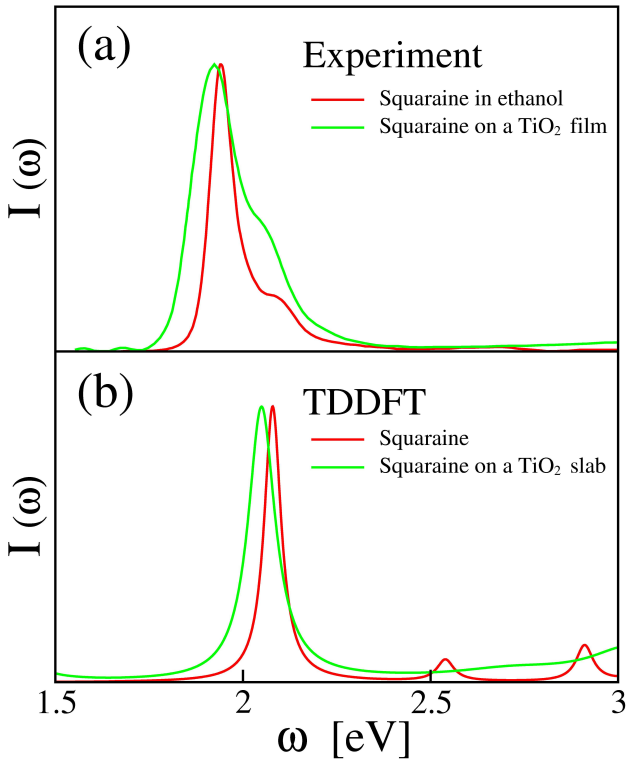

Figure 4.5: (a) Experimental absorption spectrum of squaraine in ethanol and adsorbed on a 4 μm TiO_2 film. (b) TDDFT results for the absorption spectrum of squaraine in gas-phase and adsorbed on a TiO_2 slab. The two curves have been rescaled in order to be compared.

cantly change but the main peak is broadened and the maximum in the absorption is slightly red-shifted by about 0.02 eV, due to the interaction of the anchoring group with the surface. The "shoulder" of the main peak is probably due to vibronic transitions [93]. In Fig. 4.5(b) the TDDFT results are shown for the gas-phase squaraine and for the dye+slab system models. The main transition of squaraine has been found at 2.08 eV, shifted by 0.14 eV compared to experimental results. When the molecule is adsorbed on the surface, a small red-shift of about 0.03 eV occurs, in agreement with experimental results. The "shoulder" observed in the experimental spectra is not present in our results due to our neglect of vibronic effects.

We have seen that theoretical and experimental results in the visible range are in satisfactory agreement. Both seem to suggest an indirect transition mechanism

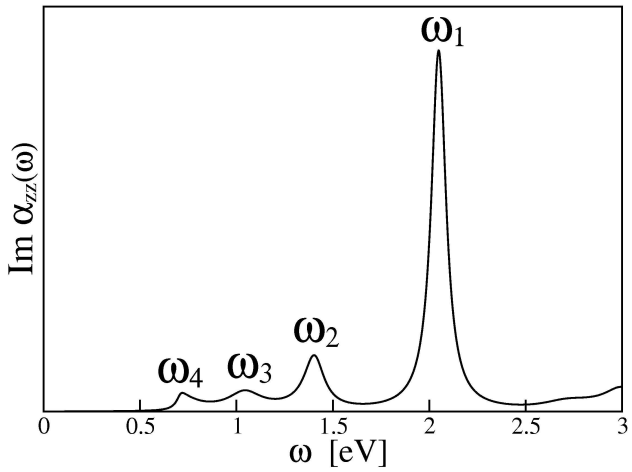

Figure 4.6: Imaginary part of the zz component of the polarizability in the energy range between 0 and 3 eV.

in the solar cell, since there is no significant change between the spectrum of free-standing and adsorbed molecules. Nevertheless we have found some weak absorption in the infrared region, namely for energies lower than the main transition peak. There is no experimental evidence of such transitions, since such energy regions have not been investigated. These transitions are showed in the zz component of the absorption (see Fig. 4.6), but they are present with smaller intensity in the yy component as well. Although the presence of these excitations does not change the prediction of the dominant transition mechanism significantly, further investigation is required to fully understand their nature.

In order to gain a better insight into the mechanism of the transition (direct or indirect), we have considered the response of the charge density to the application of a unitary external electric field along the j axis, E_j, in linear response regime: $n'_{E_j}(\mathbf{r},\omega)$. The standard batch representation of $n'_{E_j}(\mathbf{r},\omega)$ is (see Eq. (2.38)) :

$$n'_{E_j}(\mathbf{r},\omega) = 2\sum_v \phi_v(\mathbf{r}) q_v(\mathbf{r},\omega) \tag{4.1}$$

where q_v is obtained by solving the linear system (2.39) with $v_{ext} = -E_j(\omega) r_j$. Since we are interested in the transitions appearing in the zz component of the polarizability, it is enough to compute the integral of $n'_{E_j}(\mathbf{r},\omega)$ in the planes or-

thogonal to the z direction, namely

$$\bar{n}'_{E_z}(z,\omega) = \frac{1}{\Sigma_{xy}} \int n'_{E_z}(\mathbf{r},\omega) dxdy. \tag{4.2}$$

where Σ_{xy} is the area of the xy base. In Fig. 4.7 we show the values of $\mathrm{Im}\, \bar{n}'_{E_z}(z,\omega)$ for the four transitions displayed in Fig. 4.6 as a function of the z coordinate; the region of space occupied by the molecule and by the slab are delimited by green and red lines respectively. In the frame (a) of Fig. 4.6 we see a strong response of the molecule, which is very similar to the free-molecule response (blue line), and almost no response in the region of the slab, but for a charge accumulation on the surface opposite to the one where the dye is anchored. In the other frames of Fig. 4.6 the charge response function is shown for ω_2, ω_3, and ω_4. Especially considering the plots in (c) and (d), it is evident that the low energy peaks are mainly associated to a molecule-slab transition. For example in the frame (c), the density response is almost exclusively negative in the squaraine region, thus forming a net dipole between the molecule and the slab. This transition corresponds to a direct injection mechanism.

In all the response functions in Fig. 4.7, a charge accumulation in the lower surface of the slab is present. A possible explanation of such behavior is based on a classical model. Indeed we can suppose the slab to behave as a capicitor in which the dielectric material uniformly polarizes under an external electric field. In this case the external field is given by the dipole within the molecule in the frame (a) and between the molecule and the upper surface in (b), (c) and (d). The uniform polarization cancel out inside the slab but manifest itself in the lower surface.

The TDDFT analysis of the optical spectra and of the charge response functions indicates that the functioning of the squaraine solar cell, although dominated by an indirect transition, also seems to involve some weaker direct transition. This feature cannot be verified, because of the lack of experimental results in the infrared energy region. Further work is necessary to improve the reliability of TDDFT calculations on DSSC systems, especially concerning the description of the substrate. First of all a more realistic model with many layers would bring to a more appropriate description of such system; but the most important problem concern the correction of gap of $\mathrm{TiO_2}$, that we have underestimated in our calculations. To this purpose, hybrid functionals, despite a large computational cost,

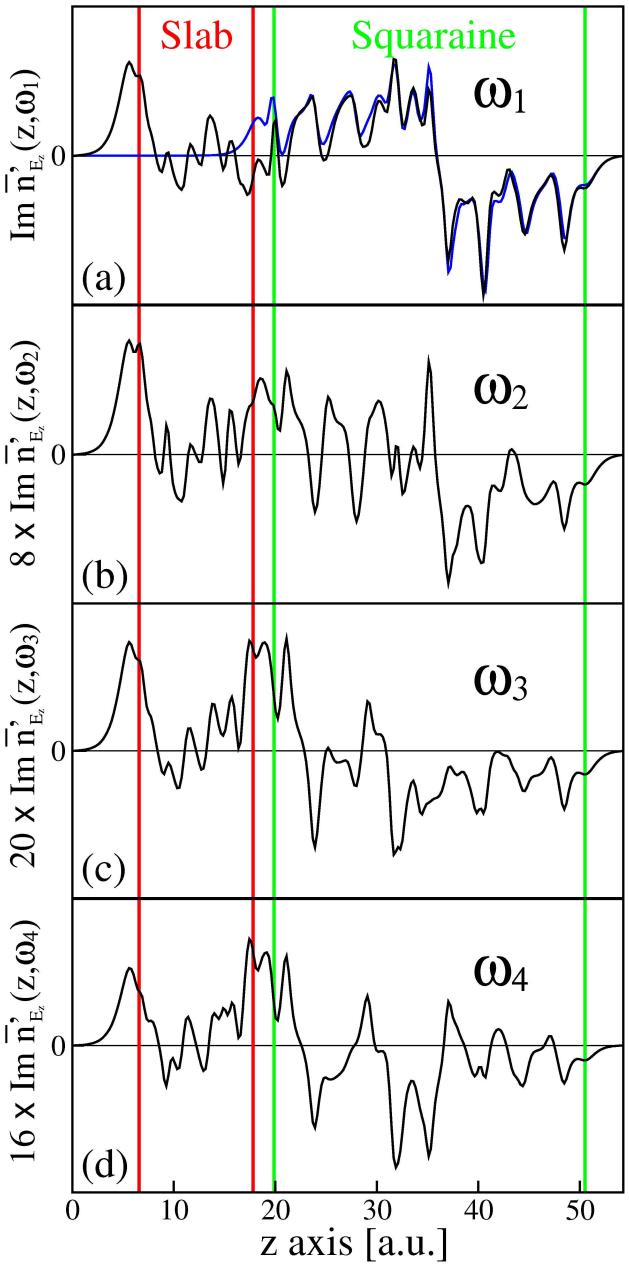

Figure 4.7: (a) Imaginary part of the charge response (4.2) for the DSSC system as a function of the z coordinate in correspondence to the energy ω_1. In blue the same quantity is shown in correspondence of the main peak (2.08 eV) of the molecule alone. The charge response for the transitions ω_2, ω_3 and ω_4 is shown in the frames (b), (c) and (d) (see Fig. 4.6). The curves have been rescaled in order to be compared.

are a suitable method to correct both the KS gap and the TDDFT optical gap of the substrate [30].

Conclusions

In this thesis a new computational approach has been introduced to solve the linearized TDDFT equations in the frequency domain. This new formulation allows one to overcome some of the drawbacks of traditional approaches, such as real-time propagations or Casida's equations. By using a super-operator formulation of linearized TDDFT, we have first represented the dynamical polarizability (but also other specific response functions) of an interacting electronic system as an off-diagonal matrix element of the resolvent of the Liouvillian super-operator. To solve the problem in practice we have used a representation for density matrices which has been borrowed from density functional perturbation theory. In this way it is possible to avoid the calculation of KS empty states, which, instead, is necessary in Casida's implementation. We have then calculated the resolvent using a newly developed algorithm based on the non-symmetric Lanczos method. The already good convergence properties of this approach have been further improved by the introduction of an inexpensive extrapolation scheme. In this way the number of iterations necessary to reach convergence ranges from few hundreds to few thousands. For this reason the numerical workload of this method is only few times larger than that needed by typical ground-state calculations for the same system. Because of the favorable computational charge, this method is particularly suitable to treat large systems, and to calculate the absorption spectrum in a wide energy range. Its reliability has been explicitly demonstrated on systems of increasing dimensions such as benzene, fullerene and chlorophyll a, obtaining optical spectra in good agreement with experiments and with more traditional TDDFT schemes. Whenever possible, comparison has shown that our approach is much more efficient than the real-time propagation of TDKS equations to calculate linear response spectra. The main advantage of our method with respect to Casida's is the possibility of calculating absorption spectra (or other dynamical

response functions) on a much broader energy range, an advantage that is shared by real-time approaches, which are however more demanding computationally.

We have also applied the newly introduced approach to a problem of remarkable applicative importance, a squaraine dye-sensitized solar cell. The results obtained are in good agreement with experiments, and it is also possible to infer the mechanism ruling the functioning of such device qualitatively.

Despite the satisfactory accuracy of the results obtained in this thesis, the main limit of our approach resides in the approximation of the xc functional used to implement it. Devising new xc functionals capable of properly describing the electron-hole interaction responsible, *e.g.*, of Rydberg and excitonic effects in the low-lying portion of the spectrum of molecular and extended systems respectively remains a major problem to be addressed and solved.

Further work is necessary in many different directions. First of all we mention the efficiency issues related to the ultrasoft implementation, particularly crucial for TDDFT applications. The computational workload of the usual reciprocal space implementation of ultrasoft pseudopotentials can be reduced of some order of magnitude by performing the same operations in real space; although this issue does not change the overall numerical scalability, it has to be addressed in order to broaden the range of applicability of the method. Secondly the method should be extended to deal with a larger range of problems, such as electron energy loss spectra and circular dichroism; in the second case it is necessary to overcome the conceptual difficulties in the definition of the angular momentum operator in periodic boundary conditions. Last but not least, new functionals should be implemented in order to overcome problems such as, e. g., the gap underestimation. Hybrids are a widespread and accurate class of functionals that improves over some of the limitations of LDA or GGA; nevertheless their use brings to implementative complications and to a larger computational workload.

Appendix A

Plane-wave pseudopotential implementation

The algorithms introduced in this thesis have been implemented as a standing alone part of the suite of codes *Quantum ESPRESSO* (see http://www.quantum-espresso.org). The TDDFT code works as post-processing application to a standard ground state calculation performed by *PWscf* (see http://www.pwscf.org/), which uses a plane-wave pseudopotential approach. This methodology is particularly suitable to treat periodic systems, but isolated systems, such as atoms and molecules, can be addressed as well by using supercells. In the plane-wave formulation the KS orbitals can be expanded as

$$\phi_{\mathbf{k}v}(\mathbf{r}) = \frac{1}{(N\Omega)^{\frac{1}{2}}} \sum_{\mathbf{G}} e^{i(\mathbf{k}+\mathbf{G})\cdot\mathbf{r}} c_v(\mathbf{k}+\mathbf{G}) \tag{A.1}$$

where Ω is the volume of the unit cell, N is the number of cells, $\mathbf{k}$ is a vector in the first Brillouin zone, $\mathbf{G}$ are the reciprocal lattice vectors and $\mathbf{c_v}(\mathbf{k}+\mathbf{G})$ are the expansion coefficients normalized to one

$$\sum_{\mathbf{G}} |c_v(\mathbf{k}+\mathbf{G})|^2 = 1. \tag{A.2}$$

The dimension of the basis set is determined by the condition

$$\frac{1}{2}|\mathbf{k}+\mathbf{G}|^2 \leq E_{cut} \tag{A.3}$$

where E_{cut} is the kinetic energy cutoff, which has to be chosen big enough to ensure accurate results. In general, for supercell calculations, $\mathbf{k}$ is set to zero,

namely only the Γ point is considered in the first Brillouin zone. Using the plane-wave expansion the KS equations can be written as

$$\sum_{\mathbf{G}'} H(\mathbf{k}+\mathbf{G},\mathbf{k}+\mathbf{G}')c_v(\mathbf{k}+\mathbf{G}') = \varepsilon_{\mathbf{k}v}c_v(\mathbf{k}+\mathbf{G}) \tag{A.4}$$

where

$$H(\mathbf{k}+\mathbf{G},\mathbf{k}+\mathbf{G}') = \frac{1}{2}|\mathbf{k}+\mathbf{G}|^2\delta_{\mathbf{G},\mathbf{G}'} + v_H(\mathbf{G}-\mathbf{G}') + v_{xc}(\mathbf{G}-\mathbf{G}') + v_{ext}(\mathbf{G},\mathbf{G}'). \tag{A.5}$$

It is important to note that the kinetic energy contribution (namely the first term of the Hamiltonian H) is diagonal in this representation. For this reason the computational cost of its application to a given vector scales linearly with the dimension of the basis set N. Unfortunately the potential terms v of Eq. (A.5) are not diagonal in this same representation but they are in the real space representation, which can be obtained performing a Fast Fourier Transform (FFT). Switching between reciprocal and real space through FFT's, the N^2 scaling of the matrix-vector product in Eq. (A.4) can be reduced to $N \log N$. Furthermore, in this way the full matrix $H(\mathbf{k}+\mathbf{G},\mathbf{k}+\mathbf{G}')$ does not need to be explicitly computed. Another advantage of the use of plane-waves is the significant simplification in the resolution of the Poisson equation, namely in the evaluation of the Hartree contribution. In reciprocal space we have simply

$$v_H(\mathbf{G}) = 2\pi \sum_{\mathbf{G}\neq 0} \frac{n(\mathbf{G})^2}{G^2} \tag{A.6}$$

which has to be Fourier transformed to real space before the application to a wave function.

These are the basic technical ingredients for a ground state DFT calculation on a plane-wave basis set. The Hamiltonian H in Eq. (A.4) is a functional of the exact ground state density and for this reason the equations have to be solved self-consistently. The first step of this procedure consists in finding a proper initial guess for the ground state density that, evaluating v_H through Eq. (A.6) and v_{xc}, can be used to build H. Solving Eq. (A.4) we obtain a new guess for the density from the KS orbitals. The procedure has to be continued until the new guess does not differ significantly from the previous one. Each self-consistent step requires the evaluation of the occupied states of H. This goal can be reached using iterative

techniques that avoid the cumbersome full diagonalization of the Hamiltonian altogether. These methods only require matrix by vector (namely Hamiltonian by wavefunction) products, which can be efficiently performed by the FFT approach described above.

In order to implement the Liouville-Lanczos equations in a plane-wave formalism the first issue is related to the evaluation of $\hat{Q}r_i\phi_v(\mathbf{r})$ in Eq. (2.40). Indeed the position operator is incompatible with the periodic boundary conditions intrinsic to the plane-wave basis set and its expectation value on wavefunctions (A.1) is ill-defined. In a perturbative regime, however, this pathology can be easily solved. Indeed what is required to calculate $\hat{Q}r_i\phi_v(\mathbf{r})$ is the evaluation of the expectation value of the position operator between an empty KS state $\phi_c(\mathbf{r})$ and an occupied state $\phi_v(\mathbf{r})$. This quantity can be expressed in periodic boundary conditions (but also in general) as

$$\langle\phi_c|r_i|\phi_v\rangle = \frac{\langle\phi_c|[H^{GS}, r_i]|\phi_v\rangle}{\varepsilon_c - \varepsilon_v}; \tag{A.7}$$

if the potential acting on the electrons is local, the commutator is simply proportional to the i^{th} component of the momentum operator. Using Eq. (A.7) we can express our desired quantity as

$$\bar{\phi_v^i}(\mathbf{r}) = \hat{Q}r_i\phi_v(\mathbf{r}) = \sum_c \phi_c(\mathbf{r})\frac{\langle\phi_c|[H^{GS}, r_i]|\phi_v\rangle}{\varepsilon_c - \varepsilon_v} \tag{A.8}$$

which can be numerically evaluated by solving the linear system

$$(H^{GS} - \varepsilon_v)|\bar{\phi_v^i}\rangle = \hat{Q}[H^{GS}, r_i]|\phi_v\rangle. \tag{A.9}$$

This operation has to be performed only once at the beginning of the calculation (clearly in case of fixed atoms).

In the Liouville-Lanczos approach the iterative procedure requires the repeated application of the Liouvillian superoperator through Eq. (2.34) and Eq. (2.35) but there are no significant differences with respect to the ground state implementation. To evaluate Eq. (2.34) we need to apply the ground state Hamiltonian to each orbital of the *batch*. This is exactly the same operation performed in iterative ground state calculations and also in this case we can take advantage of FFT techniques. The evaluation of Eq. (2.35) that we express here for the LDA case is a bit more tricky:

$$\mathcal{K}\{x_v(\mathbf{r})\} = \hat{Q}\Big[\int \frac{n'(\mathbf{r}')}{|\mathbf{r} - \mathbf{r}'|}d\mathbf{r}' + \frac{\delta v_{xc}(\mathbf{r})}{\delta n(\mathbf{r})}\Big|_{n=n_0} n'(\mathbf{r})\Big] \tag{A.10}$$

where $n'(\mathbf{r}) = \sum_v \phi_v(\mathbf{r}) x_v(\mathbf{r})$ and $\phi_v(\mathbf{r})$ are the occupied KS ground state orbitals. In Eq. (A.10) the first term can be evaluated simply by using Eq. (A.6). The second term requires the evaluation of $\frac{\delta v_{xc}(\mathbf{r})}{\delta n(\mathbf{r})}$ only once at the beginning of the TDDFT calculation, since this quantity is a functional of the ground state density only. This operation can be performed numerically using the formula

$$\frac{\delta v_{xc}(\mathbf{r})}{\delta n(\mathbf{r})} = \frac{v_{xc}[n_0(\mathbf{r}) + \epsilon n_0(\mathbf{r})](\mathbf{r}) - v_{xc}[n_0(\mathbf{r}) + \epsilon n_0(\mathbf{r})](\mathbf{r})}{2\epsilon n_0(\mathbf{r})} \tag{A.11}$$

where in the second term we explicitly wrote the functional dependence of v_{xc} on the density and where ε is a properly chosen small number. In case of GGA functionals the same evaluation leads to a more complex formalism that can be found in [99].

A relevant problem of a direct plane-wave implementation is given by the huge dimension of the basis set required to treat all the electrons explicitly. Indeed the low energy orbitals are generally localized near the nuclei; furthermore, due to the orthogonalization condition, the higher energy orbitals oscillate rapidly in that region. Fortunately the electrons lying in the inner regions are also the less involved in the chemical properties of an atom. For this reason pseudopotentials have been introduced in order to treat explicitly only the outer valence electrons and to consider the inner electrons frozen in their atomic configurations. In this approach the valence electrons move in an effective potential (the pseudopotential) which outside the core region (the dimensions have to be established in the construction of the pseudopotential) match the true potential and inside it is considerably smoother. Outside the core radius the pseudo-wave function (namely the wavefunction obtained using the pseudopotential) is only proportional to the true wavefunction. In general they are forced to be the same in the construction of the pseudopotential, which in such case is called norm-conserving. Inside the core region, instead, the pseudo-wave function is much smoother than the true wavefunction, since it is no longer necessary to ensure the orthogonalization with the core states. For this reason the total amount of required plane-waves is significantly lower.

The norm-conserving pseudopotentials in their original formulation [100, 101] are split into a local part (matching the true potential outside the core) and a non

local part for the angular momentum (vanishing outside the core):

$$v(\mathbf{r},\mathbf{r}') = v^{loc}(r)\delta(\mathbf{r}-\mathbf{r}') + \sum_{l=0}^{l_{max}} |Y_{lm}\rangle v_l^{nl}(r)\langle Y_{lm}|, \tag{A.12}$$

where Y_{lm} are the angular momentum eigenfunctions. In order to make the calculation more efficient, Kleinman and Bylander [102] introduced the separable form for the non local part

$$v(\mathbf{r},\mathbf{r}') = v^{loc}(r)\delta(\mathbf{r}-\mathbf{r}') + \sum_i \frac{|\phi_{lm}^{PS} v_l^{nl}\rangle\langle v_l^{nl}\phi_{lm}^{PS}|}{\langle\phi_{lm}^{PS}|v_l^{nl}|\phi_{lm}^{PS}\rangle} \tag{A.13}$$

which is non local also in the radial part and which reproduces the same action of the previous formula on the reference atomic pseudo-wave function ϕ_{lm}^{PS}.

The method of norm-conserving pseudopotentials has been improved by the introduction of ultrasoft pseudopotentials [103]. The formalism, which is more complex, has been considered in Appendix B for the specific case of TDDFT.

Appendix B

Ultrasoft implementation

A crucial parameter for the convergence properties of the Liouville-Lanczos method is the dimension of the basis set. For this reason to use ultrasoft pseudopotentials is fundamental, for it allows a substantial decrease in the number of necessary plane-waves at the price of some complication of the formalism [103]. The equations developed in Chapter 2 apply to all-electron as well as to calculations performed using norm-conserving pseudopotentials, which give rise to an ordinary KS ground-state eigenvalue problem. Ultrasoft pseudopotentials (USPP's), instead, give rise to a generalized KS ground-state eigenvalue problem and the TDKS equations have to be modified accordingly [77, 104]. For the sake of completeness in the following we will give a sketch of the main equations; the details of the Ultrasoft pseudopotential implementation in TDDFT are given in [77, 104].

In the framework of USPP's, the charge density is written as a sum $n(\mathbf{r},t) = n^{\text{US}}(\mathbf{r},t) + n^{\text{aug}}(\mathbf{r},t)$. The delocalized contribution, n^{US}, is represented as the sum over the squared moduli of the KS orbitals: $n^{\text{US}}(\mathbf{r},t) = \sum_v |\phi_v(\mathbf{r},t)|^2$. The *augmentation charge* n^{aug}, instead, is written in terms of so-called augmentation functions $Q^I_{nm}(\mathbf{r})$:

$$n^{\text{aug}}(\mathbf{r},t) = \sum_v \sum_{n,m,I} Q^I_{nm}(\mathbf{r}) \langle \phi_v(t)|\beta^I_n\rangle \langle \beta^I_m|\phi_v(t)\rangle. \tag{B.1}$$

The augmentation functions, as well as the functions $\beta^I_n(\mathbf{r}) \equiv \beta_n(\mathbf{r}-\mathbf{R}_I)$ are localized in the core region of atom I. Each β_n consists of an angular momentum eigenfunction times a radial function that vanishes outside the core radius. Typically one or two such functions are used for each angular momentum channel and

atom type. The indices n and m in Eq. (B.1) run over the total number of such functions for atom I. In practice, the functions $Q_{nm}(\mathbf{r})$ and $\beta_n(\mathbf{r})$ are provided with the pseudopotential for each type of atom.

The advantage of using USPP's over standard norm-conserving pseudopotentials comes from this separation of the strongly localized contributions to the charge density from the more delocalized contributions. The square moduli of the KS orbitals only represent the latter part of $n(\mathbf{r}, t)$, and therefore lower Fourier components in the representation of the orbitals are sufficient for a correct representation of the charge density. The kinetic energy cutoff that determines the size of the basis set can therefore be chosen to be much smaller in typical USPP applications than in corresponding calculations with norm-conserving PP's. The smaller basis set not only reduces the dimensions of the matrices during the computation, but it also allows for a faster convergence of spectroscopic quantities calculated with the Liouville-Lanczos technique.

The generalized expression for the USPP charge density given above entails a more complicated structure of the KS eigenvalue problem. Instead of the standard KS eigenvalue equation (1.7), one now has

$$\hat{H}_{KS}^{GS}\phi_v(\mathbf{r}) = \epsilon_v \hat{S}\phi_v(\mathbf{r}), \tag{B.2}$$

where the overlap operator $\hat{S}$ is defined as

$$\hat{S} = \hat{\mathbb{1}} + \sum_{n,m,I} q_{nm}^I |\beta_n^I\rangle\langle\beta_m^I|, \tag{B.3}$$

with $q_{nm}^I = \int d\mathbf{r}\, Q_{nm}^I(\mathbf{r})$ and $\hat{\mathbb{1}}$ the identity operator.

Consequently also the TDKS Eq. (1.18) contains the overlap operator in the USPP formalism:

$$i\hat{S}\frac{\partial\phi_v(\mathbf{r}, t)}{\partial t} = \hat{H}_{KS}(t)\phi_v(\mathbf{r}, t), \tag{B.4}$$

which can be used to modify the corresponding quantum Liouville equation (2.1) accordingly.

Using a derivation similar to that shown in Chapter 2, we arrive at a standard batch representation of the TDDFT Liouville equation in the USPP formalism. It has the same form as Eq. (2.39) above, but with the super-operators $\mathcal{D}$ and $\mathcal{K}$

replaced by

$$\mathcal{D}^{US}\{x_v(\mathbf{r})\} = \{(\hat{S}^{-1}\hat{H}^{GS}_{KS} - \epsilon_v)x_v(\mathbf{r})\} \tag{B.5}$$

$$\mathcal{K}^{US}\{x_v(\mathbf{r})\} = \left\{\hat{S}^{-1}\hat{Q}\sum_{v'}\int K_{vv'}(\mathbf{r},\mathbf{r}')x_{v'}(\mathbf{r}')d\mathbf{r}'\right\}, \tag{B.6}$$

and the right hand side of Eq. (2.39) by

$$\begin{pmatrix} 0 \\ \{\hat{S}^{-1}\hat{Q}v_{ext}(\mathbf{r})\phi_v(\mathbf{r})\} \end{pmatrix}; \tag{B.7}$$

in this case the projector $\hat{Q}$ onto the empty states manifold is given by $\hat{Q} = \hat{S} - \sum_v \hat{S}|\phi_v\rangle\langle\phi_v|$. The inverse overlap operator, $\hat{S}^{-1}$, appearing in these expressions can be cast in the form

$$\hat{S}^{-1} = \mathbb{1} + \sum_{n,m,I,J} \lambda^{IJ}_{nm}|\beta^I_n\rangle\langle\beta^J_m|, \tag{B.8}$$

which is very similar to the $\hat{S}$ operator itself, given in Eq. (B.3), except for the fact that $\hat{S}^{-1}$ generally connects β-functions localized on different atoms. The numbers λ^{IJ}_{nm} can be obtained from the condition $\hat{S}\hat{S}^{-1} = \mathbb{1}$. If the atoms are kept at fixed positions, as this is the case, the overlap operator is independent of time and the λ^{IJ}_{nm} needs to be calculated only once.

In the practical implementation of the USSP method we can take advantage of the strong spatial localization of the functions $Q_{nm}(\mathbf{r})$ and $\beta_n(\mathbf{r})$ [105]. This feature can be exploited by using a real space grid instead of using the reciprocal space representation (see Appendix A). For example, when we add the augmentation charge Eq. (B.1) to the smoother part, in reciprocal space we have to sum over all the Fourier components; in real space, instead, we have to sum over only relatively few grid points, since $Q_{nm}(\mathbf{r})$ is zero elsewhere. Similarly, to calculate $\langle\beta^I_m|\phi_v(t)\rangle$ in Eq. (B.1), in reciprocal space we have to perform the scalar product $\sum_{\mathbf{G}}\beta^I_m(\mathbf{G})\phi_v(\mathbf{G},t)$ between large dimensional reciprocal space vectors; the same quantity in real space is proportional to $\sum_i \beta^I_m(\mathbf{r}_i)\phi_v(\mathbf{r}_i,t)$, where the sum has to be performed only on the points in which $\beta^I_m(\mathbf{r})$ is non zero. The reduction of the computational workload that can be reached in these, as well as in other USPP operations, is roughly proportional to the ratio between the volume occupied by the localized functions $Q_{nm}(\mathbf{r})$ and $\beta_n(\mathbf{r})$ and the total volume of the

simulation cell. Since in a typical PW implementation it is possible to switch from reciprocal to real space through FFT (see appendix B), ultrasoft pseudopotentials can be treated on a real space grid. In general, for ground state calculations, this is not strictly necessary, and indeed in the *PWscf* this is not the standard way to proceed. In the Liouville-Lanczos approach, instead, operations relative to USPP are much more frequent, and the overall computational time is strongly influenced by this feature.

We have tested an implementation for the treatment of the augmentation charge in real space, with the specific purpose of applying this methodology in TDDFT calculations. For what concerns accuracy, we have found that, in general, the convergence of ground state total energies requires a larger charge cutoff than in standard reciprocal space calculations. Nevertheless, even using the same charge cut-off as in the reciprocal space calculation, the single occupied and empty KS eigenvalues are not significantly shifted, and the overall TDDFT spectrum converges to the proper final result. Using the real space approach, the computational cost to treat augmentation charges has decreased by some order of magnitude. For this reason, the real space technique has become a really powerful tool, which we have used to address the problem of dye-sensitized solar cells, after the tests on the previous cases. Further work is necessary to introduce a real space implementation for $\beta_n(\mathbf{r})$.

Bibliography

[1] Hohenberg, P. and Kohn, W. *Phys. Rev.* **136**, 864 (1964).

[2] Kohn, W. and Sham, L. J. *Phys. Rev.* **140**, 1133 (1965).

[3] Marques, M. A. L., Ullrich, C. A., Nogueira, F., Rubio, A., Burke, K., and Gross, E. K. U., editors. *Time-Dependent Density Functional Theory*, volume 706 of *Lecture notes in Physics*, Berlin, (2006). Springer-Verlag.

[4] Runge, E. and Gross, E. K. U. *Phys. Rev. Lett.* **52**, 997 (1984).

[5] Onida, G., Reining, L., and Rubio, A. *Rev. Mod. Phys.* **74**, 601 (2002).

[6] Bauernschmitt, R. and Ahlrichs, R. *Chem. Phys. Lett.* **256**, 454 (1996).

[7] Sundholm, D. *Chem. Phys. Lett.* **302**, 480 (1999).

[8] Sundholm, D. *Chem. Phys. Lett.* **317**, 545 (2000).

[9] Dahlbom, M. G. and Reimers, J. R. *Mol. Phys.* **103**, 1057 (2005).

[10] Linnanto, J. and Korppi-Tommola, J. *Phys. Chem. Chem. Phys.* **8**, 663 (2006).

[11] Marques, M. A. L., López, X., Varsano, D., Castro, A., and Rubio, A. *Phys. Rev. Lett.* **90**, 258101 (2003).

[12] Yabana, K. and Bertsch, G. F. *Int. J. Quantum Chem.* **75**, 55 (1999).

[13] Varsano, D., Di Felice, R., Marques, M. A. L., and Rubio, A. *J. Phys. Chem. B* **110**, 7129 (2006).

[14] Fantacci, S., De Angelis, F., Sgamellotti, A., Marrone, A., and Re, N. *J. Am. Chem. Soc.* **127**, 14144 (2005).

[15] Niehaus, T. A., Suhai, S., della Sala, F., Lugli, P., Elstner, M., Seifert, G., and Fraunheim, T. *Phys. Rev. B* **63**, 085108 (2001).

[16] Tsolakidis, A., Sanchez-Portal, D., and Martin, R. M. *Phys. Rev. B* **66**, 235416 (2002).

[17] Bauernschmitt, R., Ahlrichs, R., Hennrich, F. H., and Kappes, M. M. *J. Am. Chem. Soc.* **120**, 5052 (1998).

[18] Yabana, K. and Bertsch, G. F. *Phys. Rev. B* **54**, 4484 (1996).

[19] Blase, X. and Ordejón, P. *Phys. Rev. B* **69**, 085111 (2004).

[20] Marinopoulos, A. G., Wirtz, L., Marini, A., Olevano, V., Rubio, A., and Reining, L. *Appl. Phys. A: Materials Science & Processing* **78**, 1157–1167 (2004).

[21] Marinopoulos, A. G., Reining, L., Rubio, A., and Vast, N. *Phys. Rev. Lett.* **91**, 046402 (2003).

[22] Serra, L. and Rubio, A. *Phys. Rev. Lett.* **78**, 1428 (1997).

[23] Vasiliev, I., Öğüt, S., and Chelikowsky, J. R. *Phys. Rev. Lett.* **78**, 4805 (1997).

[24] Vasiliev, I., Öğüt, S., and Chelikowsky, J. R. *Phys. Rev. Lett.* **82**, 1919 (1999).

[25] Vasiliev, I., Öğüt, S., and Chelikowsky, J. R. *Phys. Rev. Lett.* **86**, 1813 (2001).

[26] Vasiliev, I., Öğüt, S., and Chelikowsky, J. R. *Phys. Rev. B* **65**, 115416 (2002).

[27] Idrobo, J. C., Öğüt, S., and Jellinek, J. *Phys. Rev. B* **72**, 085445 (2005).

[28] Del Puerto, M. L., Tiago, M. L., and Chelikowsky, J. R. *Phys. Rev. Lett.* **97**, 096401 (2006).

[29] Lehtonen, O. and Sundholm, D. *Phys. Rev. B* **72**, 085424 (2005).

[30] De Angelis, F., Tilocca, A., and Selloni, A. *J. Am. Chem. Soc.* **126**, 15024 (2004).

[31] Persson, P. and Lundqvist, M. J. *J. Phys. Chem. B* **109**, 11918 (2005).

[32] Furche,, F., Ahlrichs, R., Wachsmann, C., Weber, E., Sobanski, A., Vögtle, F., and Grimme, S. *J. Am. Chem. Soc.* **122**, 1717 (2000).

[33] Yabana, K. and Bertsch, G. F. *Phys. Rev. A* **60**, 1271 (1999).

[34] Reining, L., Olevano, V., Rubio, A., and Onida, G. *Phys. Rev. Lett.* **88**, 066404 (2002).

[35] Sottile, F., Olevano, V., and Reining, L. *Phys. Rev. Lett.* **91**, 056402 (2003).

[36] Adragna, G., Del Sole, R., and Marini, A. *Phys. Rev. B* **68**, 165108 (2003).

[37] Marini, A., del Sole, R., and Rubio, A. *Phys. Rev. Lett.* **91**, 256402 (2003).

[38] Marini, A. and Rubio, A. *Phys. Rev. B* **70**, 081103 (2004).

[39] Botti, S., Sottile, F., Vast, N., Olevano, V., Reining, L., Weissker, H.-C., Rubio, A., Onida, G., Del Sole, R., and Godby, R. W. *Phys. Rev. B* **69**, 155112April.

[40] Del Sole, R., Adragna, G., Olevano, V., and Reining, L. *Phys. Rev. B* **67**, 045207 (2003).

[41] Burke, K., Werschnik, J., and Gross, E. K. U. *J. Chem. Phys.* **123**, 062206 (2005).

[42] Langreth, D. C. and Perdew, J. P. *Solid State Commun.* **17**, 1425 (1975).

[43] Gunnarsson, O. and Lundqvist, B. I. *Phys. Rev. B* **13**, 4274 (1976).

[44] Kohn, W., Meir, Y., and Makarov, D. E. *Phys. Rev. Lett.* **80**, 4153 (1998).

[45] Lein, M., Gross, E. K. U., and Perdew, J. P. *Phys. Rev. B* **61**, 13431 (2000).

[46] Furche, F. and van Voorhis, T. *J. Chem. Phys.* **122**, 164106 (2005).

[47] Marini, A., García-González, P., and Rubio, A. *Phys. Rev. Lett.* **96**, 136404 (2006).

[48] Petersilka, M., Gossmann, U. J., and Gross, E. K. U. *Phys. Rev. Lett.* **76**, 1212 (1996).

[49] Casida, M. In *Recent Advances in Density Functional Methods, Part I,* Chong, P., editor, 155 (World Scientific, Singapore, 1995).

[50] Jørgensen, P., Jensen, H. J. A., and Olsen, J. *J. Chem. Phys.* **89**, 3654 (1988).

[51] Stratmann, R. E., Scuseria, G. E., and Frisch, M. J. *J. Chem. Phys.* **109**, 8218 (1998).

[52] Baroni, S., Giannozzi, P., and Testa, A. *Phys. Rev. Lett.* **58**, 1861 (1987).

[53] Baroni, S., de Gironcoli, S., Dal Corso, A., and Giannozzi, P. *Rev. Mod. Phys.* **73**, 515 (2001).

[54] Hutter, J. *J. Chem. Phys.* **118**, 3928 (2003).

[55] O'Regan, B. and Grätzel, M. *Nature* **53**, 737 (1991).

[56] Martin, R. M. *Electronic Structure*. Cambridge University Press, Cambridge, first edition (2004).

[57] Ceperley, D. M. and Alder, B. J. *Phys. Rev. Lett.* **45**, 566 (1980).

[58] Vosko, S. H., Wilk, L., and Nusair, M. *Can. J. Phys.* **58**, 1200 (1980).

[59] Perdew, J. P. and Zunger, A. *Phys. Rev. B* **23**, 5048 (191).

[60] Becke, A. D. *Phys. Rev. A* **38**, 3098 (1988).

[61] Perdew, J. P. and Wang, Y. *Phys. Rev. B* **45**, 13244 (1992).

[62] Perdew, J. P., Burke, K., and Ernzerhof, M. *Phys. Rev. Lett.* **77**, 3865 (1996).

[63] Fetter, A. L. and Walecka, J. D. *Quantum Theory of Many-Particle Systems*. McGraw-Hill, New York, first edition, (1971).

[64] Davidson, E. R. *J. Comp. Phys.* **17**, 87 (1975).

[65] Baerends, E. J., Ellis, D. E., and Ros, P. *Chem. Phys.* **2**, 41 (1973).

[66] Koonin, S. E. and Meredith, D. C. *Computational Physics*. Addison Wesley, Menlo Park, CA, first edition, (1990).

[67] Car, R. and Parrinello, M. *Phys. Rev. Lett.* **55**, 2471 (1985).

[68] Furche, F. *Journal of Chemical Physics* **114**, 5982 (2001).

[69] Saad, Y. *Iterative Methods for Sparse Linear Systems*. SIAM, Philadelphia, second edition, (2003).

[70] Haydock, R., Heine, V., and Kelly, M. J. *J. Phys. C* **5**, 2845 (1972).

[71] Haydock, R., Heine, V., and Kelly, M. J. *J. Phys. C* **8**, 2591 (1975).

[72] Bullet, D. W., Haydock, R., Heine, V., and Kelly, M. volume 35 of *Solid State Physics*. Academic Press, New York (1980).

[73] Grosso, G. and Pastori Parravivicini, G. *Memory function approaches to stochastic problems in condensed matter*, chapter Memory function methods in solid state physics, 133–181. John Wiley and Sons (1985).

[74] Golub, G. H. and Loan, C. F. V. *Matrix Computations*. Johns Hopkins University Press, Baltimore, MD, 3rd edition, (1996).

[75] Walker, B., Saitta, A. M., Gebauer, R., and Baroni, S. *Phys. Rev. Lett.* **96**, 113001 (2006).

[76] Marques, M. A. L., Castro, A., Bertsch, G. F., and Rubio, A. *Comp. Phys. Commun.* **151**, 60 (2003).

[77] Qian, X., Li, J., Lin, X., and Yip, S. *Phys. Rev. B* **73**, 035408 (2006).

[78] Parlett, B. N., Taylor, D. R., and Liu, Z. A. *Mathematics of Computation* **44**, 105 (1985).

[79] Freund, R. W., Gutknecht, M. H., and Nachtigal, N. M. *SIAM J. Sci. Stat. Comput.* **14**, 470 (1993).

[80] Cullum, J., Kerner, W., and Willoughby, R. *Comp. Phys. Commun.* **53** (1989).

[81] Turchi, P., Ducastelle, F., and Treglia, G. *J. Phys. C* **15**, 2891 (1982).

[82] Leach, S., Vervloet, R., Despres, A., Breheret, E., Hare, J. P., Dennis, T. J., Taylor, R., and Walton, D. R. M. *Chem. Phys.* **160**, 451 (1992).

[83] Gouterman, M. *J. Mol. Spectrosc.* **6**, 138 (1961).

[84] Linnanto, J. and Korppi-Tommola, J. *Phys. Chem. Chem. Phys.* **2**, 4962 (2000).

[85] Cai, Z. L., Crossley, M. J., Reimers, J. R., Kobayashi, R., and Amos, R. D. *J. Phys. Chem. B* **110**, 15624 (2006).

[86] Du, H., Fuh, R. C. A., Li, J., Corkan, L. A., and Lindsey, J. S. *Photochem. Photobio.* **68**, 141 (1998).
http://omlc.ogi.edu/spectra/PhotochemCAD/html/index.html.

[87] Nazeeruddin, M. K., Kay, A., Rodicio, I., Humphry-Baker, R., Muller, E., Liska, P., Vlachopoulos, N., and Grätzel, M. *J. Am. Chem. Soc.* **115**, 6382 (1993).

[88] Grätzel, M. *Nature* **414**, 338 (2001).

[89] Li, C., Wang, W., Wang, X., Zhang, B., and Cao, Y. *Chem. Lett.* **34**, 554 (2005).

[90] Alex, S., Santhosh, U., and Das, S. J. *Photochem. Photobiol. A* **172**, 65 (2005).

[91] Chen, Y., Zeng, Z., Li, C., Wang, W., Wang, X., and B., Z. *New J. Chem.* **29**, 773 (2005).

[92] Otsuka, A., Funabiki, K., Sugiyama, N., Yoshida, T., Minoura, M., and Matsui, M. *Chem. Lett.* **35**, 666 (2006).

[93] Burke, A., Schmidt-Mende, L., Ito, S., and Grätzel, M. *Chem. Commun.* , 234 (2007).

[94] Yum, J., Walter, P., Huber, S., Rentsch, D., Geiger, T., Nüesch, P., De Angelis, F., Grätzel, M., and Nazeeruddin, M. K. *J. Am. Chem. Soc.* **115**, 6382 (1993).

[95] Zhao, W., Hou, Y. J., Wang, X. S., Zhang, B. W., Cao, Y., Yang, R., Wang, W. B., and R., X. X. *Solar Energy Materials and Solar Cells* **58**, 173 (1999).

[96] Park, N.-G., van de Lagemaat, J., and Frank, A. J. *J. Phys. Chem. B* **104**, 8989 (2000).

[97] Wang, Z.-S., Kawauchi, H., Kashima, T., and Arakawa, H. *Coord. Chem. Rev.* **248**, 1381 (2004).

[98] Stampfl, C. and Van de Walle, C. G. *Phys. Rev. B* **59**, 5521 (1999).

[99] Dal Corso, A. and de Gironcoli, S. *Phys. Rev. B* **62**, 273 (2000).

[100] Hamann, D. R., Schlüter, M., and Chiang, C. *Phys. Rev. Lett.* **43**, 1494 (1979).

[101] Bachelet, G. B., Hamann, D. R., and Schlüter, M. *Phys. Rev. B* **26**, 4199 (1982).

[102] Kleinman, L. and Bylander, D. M. *Phys. Rev. Lett.* **48**, 1425 (1982).

[103] Vanderbilt, D. *Phys. Rev. B* **41**, 7892 (1990).

[104] Walker, B. and Gebauer, R. . Accepetd for publication in J. Chem. Phys.

[105] Laasonen, K., Pasquarello, A., Car, R., Lee, C., and Vanderbilt, D. *Phys. Rev. B* **47**, 10142 (1993).

Acknowledgements

I would like to thank my supervisors, Stefano Baroni and Ralph Gebauer, for having offered me the opportunity to do this work, for many useful suggestions and for their support.

I am thankful to Filippo De Angelis for the fruitful collaboration that has led to part of the work in this thesis and for many useful hints to my work.

I am also indebted with Brent Walker for having introduced me to the practical aspects of the work done in this thesis.

The help of Stefano de Gironcoli and Andrea Dal Corso has been essential to solve many technical and conceptual issues.

I thank Yousef Saad for discussions and suggestions about the mathematical aspects of the problems I studied.